MANTRA: An Integral Reactor Physics Experiment to Infer the Neutron Capture Cross Sections of Actinides and Fission Products in Fast and Epithermal Spectra

FY15 Report

October 2015

Idaho National Laboratory

MANTRA: An Integral Reactor Physics Experiment to Infer the Neutron Capture Cross Sections of Actinides and Fission Products in Fast and Epithermal Spectra

FY15 Report

ISU PI: G. Imel

INL PI: G. Youinou

Senior Advisors: M. Salvatores, G. Palmiotti

ATR-NSUF: D. Ogden (NSUF Program Manager), T. Maddock (Experiment Manager)

Neutronics Analyses: C. Glass (pre-irradiation analyses), J. Sterbentz, G. Palmiotti & J. K. Nimmagada (post-irradiation analyses)

Pre-irradiation Thermal Analyses: P. Murray, W. Jones

Mechanical Design: H. Veselka

ATR Irradiation: B. Horkley

Post Irradiation Examination: J.Berg, J. Giglio, T. Giglio, J. Sommers, B. Storms

Table of Contents

1. INTRODUCTION

Neutron cross-sections characterize the way neutrons interact with matter. They are essential to most nuclear engineering projects and, even though theoretical progress has been made as far as the predictability of neutron cross-section models, measurements are still indispensable to meet tight design requirements for reduced uncertainties. Within the field of fission reactor technology, one can identify the following specializations that rely on the availability of accurate neutron cross-sections: (1) fission reactor design, (2) nuclear fuel cycles, (3) nuclear safety, (4) nuclear safeguards, (5) reactor monitoring and neutron fluence determination and (6) waste disposal and transmutation.

In particular, the assessment of advanced fuel cycles requires an extensive knowledge of transuranics cross sections. Plutonium isotopes, but also Americium, Curium and up to Californium isotope data are required with a small uncertainty in order to optimize significant features of the fuel cycle that have an impact on feasibility studies (e.g. neutron doses at fuel fabrication, decay heat in a repository etc.).

Different techniques are available to determine neutron cross-sections experimentally with the common denominator that a source of neutrons is necessary. It can either come from an accelerator that produces neutrons as a result of interactions between charged particles and a target or it can come from a nuclear reactor. When the measurements are performed with an accelerator, they are referred to as *differential* since the analysis of the data provides the cross-sections for different discrete energies, i.e. $\sigma(E_i)$, and for the diffusion cross-sections for different discrete angles.

Another approach is to irradiate a very pure sample in a test reactor such as the Advanced Test Reactor (ATR) at INL and, after a given time, determine the amount of the different transmutation products. The precise characterization of the nuclide densities before and after neutron irradiation allows to infer energy-integrated neutron cross-sections, i.e. $\int_0^\infty \sigma(E)\varphi(E)\,dE$, where $\varphi(E)$ is the neutron flux "seen" by the sample. This approach which is usually defined and led by reactor physicists is referred to as *integral* and is the object of this report.

These two sources of information, i.e. differential and integral, are complementary and are used by the nuclear physicists in charge of producing the evaluated nuclear data files used by the nuclear community (ENDF, JEFF…). The generation of accurate nuclear data files requires an iterative process involving reactor physicists and nuclear data evaluators such as illustrated in Figure 1.1. This experimental program has been funded by the ATR National Scientific User Facility (ATR-NSUF) and by the DOE Office of Science in the framework of the Recovery Act. It has been given the name MANTRA for Measurement of Actinides Neutron TRAnsmutation.
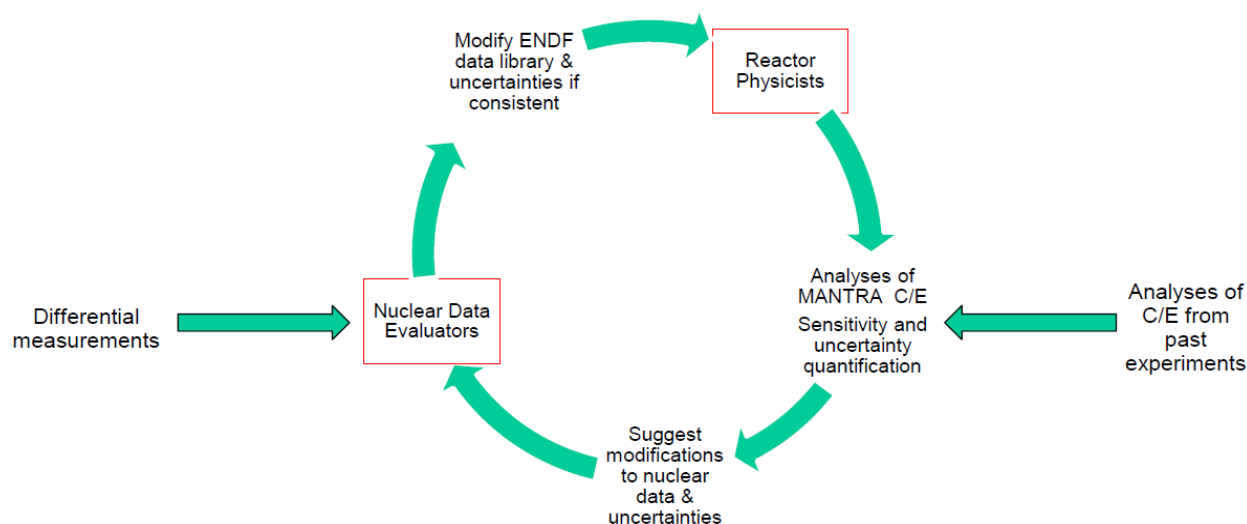

Figure 1.1. Iterative process necessary to generate accurate nuclear data files

2. GENERAL PRINCIPLES OF NEUTRON CROSS-SECTIONS DETERMINATION THROUGH SAMPLES IRRADIATION

2.1. Nuclides transmutation equations

If a sample containing an isotope of mass number A and atomic number Z is irradiated in a neutron field in position $\vec{r}_s$, heavier nuclides of mass number A+1, A+2,…. will be produced as a result of successive neutron captures and beta decays. As long as no natural decay occurs, the element, i.e. Z, stays the same and the atom densities of the A+1, A+2… are given by the following set of coupled equations:

$$\frac{dN_A^Z(\vec{r}_s, t)}{dt} = -N_A^Z(\vec{r}_s, t) \, \tilde{\sigma}_{A,Z}^a(\vec{r}_s, t) \, \phi(\vec{r}_s, t)$$

$$\frac{dN_{A+1}^Z(\vec{r}_s, t)}{dt} = +N_A^Z(\vec{r}_s, t) \, \bar{\sigma}_{A,Z}^c(\vec{r}_s, t) \, \phi(\vec{r}_s, t) - N_{A+1}^Z(\vec{r}_s, t) \, \tilde{\sigma}_{A+1,Z}^a(\vec{r}_s, t) \, \phi(\vec{r}_s, t)$$

$$\frac{dN_{A+2}^Z(\vec{r}_s, t)}{dt} = +N_{A+1}^Z(\vec{r}_s, t) \, \bar{\sigma}_{A+1,Z}^c(\vec{r}_s, t) \, \phi(\vec{r}_s, t) - N_{A+2}^Z(\vec{r}_s, t) \, \tilde{\sigma}_{A+2,Z}^a(\vec{r}_s, t) \, \phi(\vec{r}_s, t)$$

$$\frac{dN_{A+3}^Z(\vec{r}_s, t)}{dt} = +N_{A+2}^Z(\vec{r}_s, t) \, \bar{\sigma}_{A+2,Z}^c(\vec{r}_s, t) \, \phi(\vec{r}_s, t) - N_{A+3}^Z(\vec{r}_s, t) \, \tilde{\sigma}_{A+3,Z}^a(\vec{r}_s, t) \, \phi(\vec{r}_s, t)$$

… … … …

where $\phi(\vec{r}_s, t) = \int \varphi(E, \vec{r}_s, t) \, dE$ is the energy-integrated time-dependant neutron flux in the sample and $\bar{\sigma}_{A+k}^c(\vec{r}_s, t) = \frac{\int \sigma_{A+k}^c(E, \vec{r}_s) \varphi(E, \vec{r}_s, t) dE}{\int \varphi(E, \vec{r}_s, t) dE}$ is the effective one-group capture cross-section. The integral in energy is carried out over the whole neutron spectrum, i.e. from about 20 MeV down to 0 eV. Finally, $\tilde{\sigma}_{A+k}^a = \bar{\sigma}_{A+k}^a + \frac{\lambda_{A+k}}{\phi} = \bar{\sigma}_{A+k}^c + \bar{\sigma}_{A+k}^f + \frac{\lambda_{A+k}}{\phi}$ takes into account the neutron absorption (essentially capture and fission) as well as natural decay. The other reactions like (n,2n), (n,3n),…or alpha decays have only an insignificant impact on the evolution of the nuclide densities and can be neglected when determining the A+1, A+2, A+3… nuclide densities.

If somewhere along the chain there is a beta decay, the element will change, i.e. Z will change into Z+1. The most important such occurrence for reactor operation is that of U-238 which after one neutron capture followed by two beta decays is transmuted into Pu-239. The corresponding equations are the following:

$$\frac{dN_{238}^{92}(\vec{r}_s, t)}{dt} = -N_{238}^{92}(\vec{r}_s, t) \, \tilde{\sigma}_{238,92}^a(\vec{r}_s, t) \, \phi(\vec{r}_s, t)$$

$$\frac{dN_{239}^{92}(\vec{r}_s, t)}{dt} = +N_{238}^{92}(\vec{r}_s, t) \, \bar{\sigma}_{238,92}^c(\vec{r}_s, t) \, \phi(\vec{r}_s, t) - N_{239}^{92}(\vec{r}_s, t) \, \tilde{\sigma}_{239,92}^a(\vec{r}_s, t) \, \phi(\vec{r}_s, t)$$

$$\frac{dN_{239}^{93}(\vec{r}_s, t)}{dt} = +\lambda_{239,92}^{\beta} N_{239}^{92}(\vec{r}_s, t) - N_{239}^{93}(\vec{r}_s, t) \, \tilde{\sigma}_{239,93}^a(\vec{r}_s, t) \, \phi(\vec{r}_s, t)$$

$$\frac{dN_{239}^{94}(\vec{r}_s, t)}{dt} = +\lambda_{239,93}^{\beta} N_{239}^{93}(\vec{r}_s, t) - N_{239}^{94}(\vec{r}_s, t) \, \tilde{\sigma}_{239,94}^a(\vec{r}_s, t) \, \phi(\vec{r}_s, t)$$

The (simplified) neutron-induced transmutation chain from U-235 to Cf-252 is shown in <u>Figure 2.1</u>.
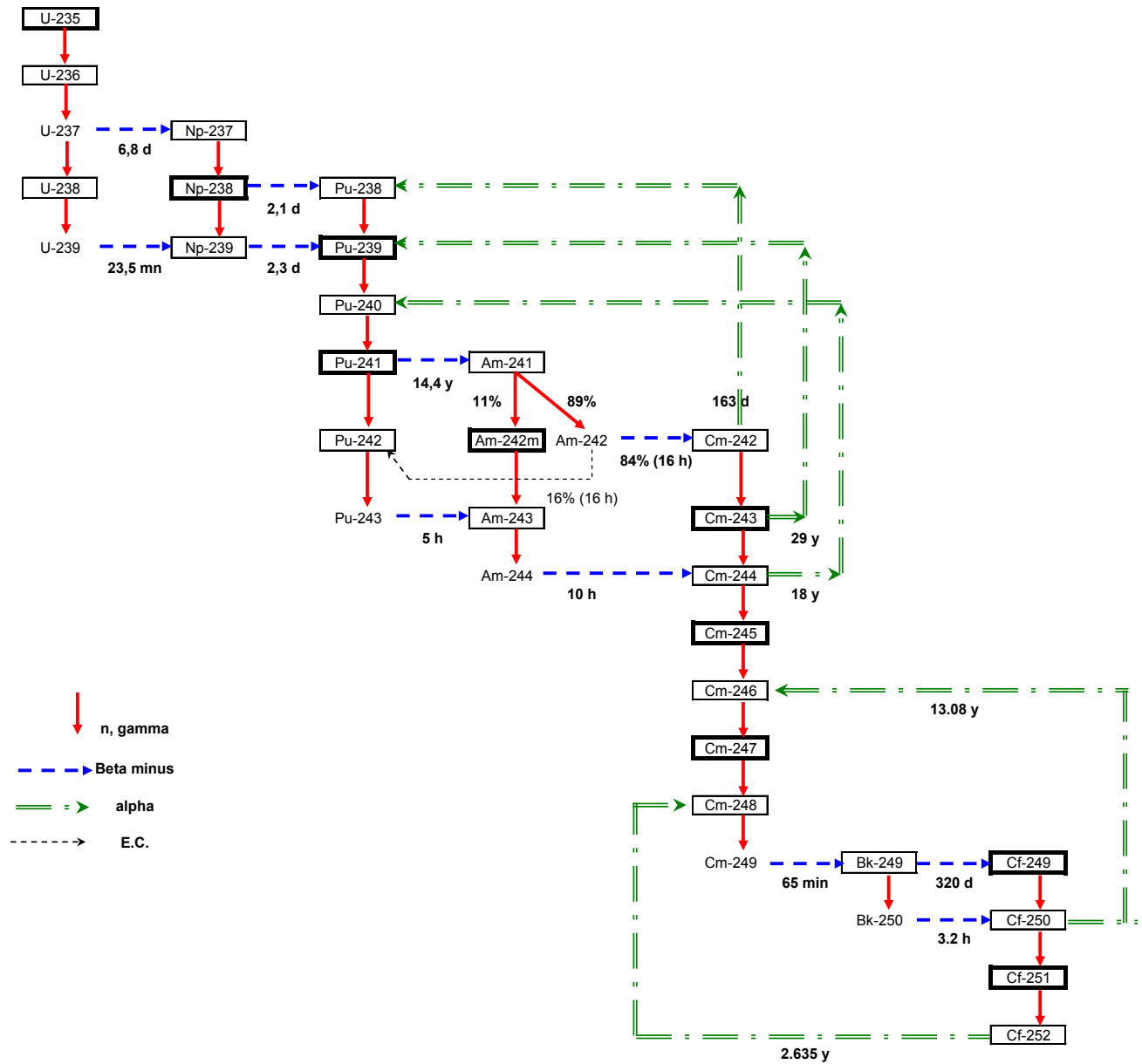
Figure 2.1. A simplified version of the neutron-induced transmutation chain from U-235 to Cf-252.

N.B.: The percentage of neutron captures on Am-241 leading respectively to Am-242m and Am-242 (i.e. the branching ratio) is energy dependent. The values of 11%-89% quoted in the figure correspond to that of a thermal neutron spectrum. The branching ratio corresponding to the subsequent natural decay of Am-242 is not energy-dependent.

The above sets of equations are actually the linearized approximation to the transmutation equations since, in principle, they are non-linear. Indeed, the neutron flux and consequently the effective one-group cross-sections can potentially depend on the nuclide densities through the resonance self-shielding phenomena and through the direct effect of the nuclide densities on the neutron spectrum. However, if the nuclide densities are small enough that they do not affect the neutron flux then the non-linearity disappears. If it is not the case the time interval under consideration has to be decomposed into smaller time steps into which the problem is supposed to be linear.

In order to facilitate the interpretation of this kind of experiment it is better if nothing perturb the neutron spectrum in the samples during the irradiation. If this is the case, the time dependence of the neutron

flux can then be factorized as $\varphi(E,\vec{r}_s,t) = \omega(E,\vec{r}_s)f(t)$ which means that the energy distribution of the neutrons, $\omega(E,\vec{r}_s)$, is time-independent and $f(t)$ is merely a normalization function taking into account local flux level variations due either to total core power fluctuations or flux tilts caused by movements of control mechanisms. Since the flux $\varphi(E,\vec{r}_s,t)$ appears both at the numerator and the denominator of the expression giving the effective one-group cross-sections, the time-dependence vanishes and it comes that:

$$\bar{\sigma}^c_{A+k}(\vec{r}_s) = \frac{\int \sigma^c_{A+k}(E,\vec{r}_s)\omega(E,\vec{r}_s)dE}{\int \omega(E,\vec{r}_s)dE}$$

With the neglect of the time-dependence of the effective one-group cross-sections, the general solution to the transmutation equations is as follows (the variable $\vec{r}_s$ has been omitted for purpose of clarity):

$$N^Z_A(T) = N^Z_A(0)e^{-\tilde{\sigma}^a_A \bar{\phi} T}$$

$$N^{Z+m}_{A+n}(T) = N^Z_A(0) \prod_{j=0}^{j=n-1} \bar{\sigma}^c_{A+j} \sum_{k=0}^{k=n} \frac{e^{-\tilde{\sigma}^a_{A+k}\bar{\phi}T}}{\prod_{t=0}^{t=n,t\neq k}(\tilde{\sigma}^a_{A+t} - \tilde{\sigma}^a_{A+k})}$$

$$\bar{\phi} = \frac{\int_0^T \phi(t)dt}{T}$$

The superscript m is equal to the number of beta decay occurring between the initial nuclide (A, Z) and the nuclide ($A+n$, $Z+m$), i.e. if no beta decay occurs then $m = 0$ whereas if one beta decay occurs then $m = 1$… The above expression for $N^{Z+m}_{A+n}(T)$ can account for beta decays simply by setting $\bar{\sigma}^c = \frac{\lambda^\beta}{\bar{\phi}}$ where necessary. The first non-zero Taylor development terms of these expressions are as follows:

$$N^Z_A(T) \sim N^Z_A(0)[1 - \tilde{\sigma}^a_A \bar{\phi} T]$$

$$N^{Z+m}_{A+n}(T) \sim \frac{1}{n!} N^Z_A(0) \left(\prod_{j=0}^{j=n-1} \bar{\sigma}^c_{A+j} \right) [\bar{\phi}T]^n$$

$$\bar{\phi} = \frac{\int_0^T \phi(t)dt}{T}$$

This shows that, as long as the product of the absorption cross-section by the time-integrated flux is small enough that the Taylor developments are legitimate, then (1) only the capture cross-sections play a role in the build-up of actinides and (2) the $A+n$ atom density increases with the nth power of the time-integrated flux.

As an example, and in the case where no beta decay occurs, the expressions for the A+1, A+2 and A+3 atom densities are as follows (the superscript Z has been omitted for purpose of clarity):

$$N_{A+1}(T) = N_A(0)\bar{\sigma}^c_A \left(\frac{e^{-\tilde{\sigma}^a_A \bar{\phi}T}}{\tilde{\sigma}^a_{A+1} - \tilde{\sigma}^a_A} + \frac{e^{-\tilde{\sigma}^a_{A+1}\bar{\phi}T}}{\tilde{\sigma}^a_A - \tilde{\sigma}^a_{A+1}} \right) \sim N_A(0)\bar{\sigma}^c_A \bar{\phi} T$$

$$N_{A+2}(T) = N_A(0)\bar{\sigma}^c_A \bar{\sigma}^c_{A+1} \left(\frac{e^{-\tilde{\sigma}^a_A \bar{\phi}T}}{(\tilde{\sigma}^a_{A+1} - \tilde{\sigma}^a_A)(\tilde{\sigma}^a_{A+2} - \tilde{\sigma}^a_A)} + \frac{e^{-\tilde{\sigma}^a_{A+1}\bar{\phi}T}}{(\tilde{\sigma}^a_A - \tilde{\sigma}^a_{A+1})(\tilde{\sigma}^a_{A+2} - \tilde{\sigma}^a_{A+1})} \right.$$
$$\left. + \frac{e^{-\tilde{\sigma}^a_{A+2}\bar{\phi}T}}{(\tilde{\sigma}^a_A - \tilde{\sigma}^a_{A+2})(\tilde{\sigma}^a_{A+1} - \tilde{\sigma}^a_{A+2})} \right) \sim \frac{1}{2} N_A(0)\bar{\sigma}^c_A \bar{\sigma}^c_{A+1}[\bar{\phi}T]^2$$

$$N_{A+3}(T)$$

$$= N_A(0)\bar{\sigma}_A^c\bar{\sigma}_{A+1}^c\bar{\sigma}_{A+2}^c \left(\frac{e^{-\tilde{\sigma}_A^a\bar{\phi}T}}{(\tilde{\sigma}_{A+1}^a - \tilde{\sigma}_A^a)(\tilde{\sigma}_{A+2}^a - \tilde{\sigma}_A^a)(\tilde{\sigma}_{A+3}^a - \tilde{\sigma}_A^a)} + \frac{e^{-\tilde{\sigma}_{A+1}^a\bar{\phi}T}}{(\tilde{\sigma}_A^a - \tilde{\sigma}_{A+1}^a)(\tilde{\sigma}_{A+2}^a - \tilde{\sigma}_{A+1}^a)(\tilde{\sigma}_{A+3}^a - \tilde{\sigma}_{A+1}^a)} + \right.$$
$$\left. \frac{e^{-\tilde{\sigma}_{A+2}^a\bar{\phi}T}}{(\tilde{\sigma}_A^a - \tilde{\sigma}_{A+2}^a)(\tilde{\sigma}_{A+1}^a - \tilde{\sigma}_{A+2}^a)(\tilde{\sigma}_{A+3}^a - \tilde{\sigma}_{A+2}^a)} + \frac{e^{-\tilde{\sigma}_{A+3}^a\bar{\phi}T}}{(\tilde{\sigma}_A^a - \tilde{\sigma}_{A+3}^a)(\tilde{\sigma}_{A+1}^a - \tilde{\sigma}_{A+3}^a)(\tilde{\sigma}_{A+2}^a - \tilde{\sigma}_{A+3}^a)} \right)$$

$$\sim \frac{1}{6} N_A(0)\bar{\sigma}_A^c\bar{\sigma}_{A+1}^c\bar{\sigma}_{A+2}^c[\bar{\phi}T]^3$$

The values obtained with the exact expressions and those obtained with the Taylor developments are compared in the tables below for two ATR experimental configurations very similar to the actual MANTRA experiment (see section 4 for more detail). These comparisons show that after 200 days of irradiation in a hard boron filtered neutron spectrum, the maximum difference between the exact and the Taylor expressions is only 1.57% proving the validity of using the Taylor. With a cadmium filter the reaction rates are more important and, as a consequence, the differences between the exact and the Taylor expressions are larger and up to 10.7% for the Pu-240 sample after 50 days of irradiation.

Table 2.1: Atom densities calculated with the exact expressions and the Taylor expansions for a pure Pu-239 sample irradiated 200 days – Boron filter – $\Phi = 5.8\ 10^{13}$ n.cm^{-2}.s^{-1}

	Pu9	Pu0	Pu1	Pu2	Am3
Exact	9.970E-01	5.996E-04	2.986E-07	6.096E-11	5.271E-15
Taylor Dev	9.970E-01	6.010E-04	3.021E-07	6.150E-11	5.310E-15
	0.000%	-0.24%	-1.15%	-0.89%	-0.74%

Table 2.2: Atom densities calculated with the exact expressions and the Taylor expansions for a pure Pu-240 sample irradiated 200 days – Boron filter – $\Phi = 5.8\ 10^{13}$ n.cm^{-2}.s^{-1}

	Pu0	Pu1	Pu2	Am3	Cm4
Exact	9.982E-01	9.895E-04	3.037E-07	3.504E-11	6.496E-15
Taylor Dev	9.982E-01	1.005E-03	3.070E-07	3.534E-11	6.570E-15
	0.000%	-1.57%	-1.08%	-0.84%	-1.12%

Table 2.3: Atom densities calculated with the exact expressions and the Taylor expansions for a pure Pu-242 sample irradiated 200 days – Boron filter – $\Phi = 5.8\ 10^{13}$ n.cm^{-2}.s^{-1}

	Pu2	Am3	Cm4	Cm5	Cm6
Exact	9.991E-01	3.450E-04	1.274E-07	2.282E-11	3.314E-15
Taylor Dev	9.991E-01	3.454E-04	1.284E-07	2.299E-11	3.337E-15
	0.000%	-0.11%	-0.82%	-0.72%	-0.71%

Table 2.4: Atom densities calculated with the exact expressions and the Taylor expansions for a pure Pu-239 sample irradiated 50 days – Cadmium filter – $\Phi = 1.5\ 10^{14}$ n.cm^{-2}.s^{-1}

	Pu9	Pu0	Pu1	Pu2	Am3	Cm4
Exact	9.832E-01	6.006E-03	6.051E-04	1.310E-06	1.211E-08	1.238E-10
Taylor Dev	9.831E-01	6.675E-03	6.563E-04	1.406E-06	1.294E-08	1.315E-10
	0.014%	-10.0%	-7.80%	-6.78%	-6.43%	-5.81%

Table 2.5: Atom densities calculated with the exact expressions and the Taylor expansions for a pure Pu-240 sample irradiated 50 days – Cadmium filter – Φ = 1.5 10^{14} n.cm^{-2}.s^{-1}

	Pu0	Pu1	Pu2	Am3	Cm4	Cm5
Exact	8.212E-01	1.756E-01	5.785E-04	7.167E-06	9.197E-08	3.889E-10
Taylor Dev	8.031E-01	1.967E-01	6.317E-04	7.755E-06	9.849E-08	4.137E-10
	2.26%	-10.7%	-8.43%	-7.58%	-6.62%	-6.00%

Table 2.6: Atom densities calculated with the exact expressions and the Taylor expansions for a pure Pu-242 sample irradiated 50 days – Cadmium filter – Φ = 1.5 10^{14} n.cm^{-2}.s^{-1}

	Pu2	Am3	Cm4	Cm5	Cm6	Cm7
Exact	9.637E-01	3.524E-02	9.003E-04	6.320E-06	5.343E-09	3.872E-12
Taylor Dev	9.630E-01	3.683E-02	9.354E-04	6.549E-06	5.502E-09	4.000E-12
	0.070%	-4.30%	-3.75%	-3.49%	-2.88%	-3.19%

As will be shown in section 3, the expressions derived for the uncertainty quantification are based on Taylor developments of the exact analytical expressions obtained for the A, A+1, A+2…atom densities as a function of time. For the purpose of uncertainty quantification, more than the values of the function themselves, it is important that the partial derivatives (i.e. the sensitivities) be well reproduced. The sensitivities of the atom densities in a Pu-240 sample with regard to the irradiation time and to the Pu-240 and Pu-241 capture cross-sections calculated with the exact and Taylor expressions agree rather well (Tables 2.7 to 2.9) which prove the validity of using the Taylor expressions for uncertainty quantification.

Table 2.7: Sensitivities of the atom densities with regard to the irradiation time calculated with the exact and Taylor expressions for a pure Pu-240 sample – Cadmium filter – Φ = 1.5 10^{14} n.cm^{-2}.s^{-1}

	Pu0	Pu1	Pu2	Am3	Cm4	Cm5
	Exact					
T_{Ref} = 50 days	8.212E-01	1.756E-01	5.785E-04	7.167E-06	9.197E-08	3.889E-10
T_{Ref} + 10%	8.052E-01	1.910E-01	6.939E-04	9.465E-06	1.337E-07	6.225E-10
	-2.0%	8.8%	19.9%	32.1%	45.4%	60.1%
	Taylor					
T_{Ref} = 50 days	8.031E-01	1.967E-01	6.317E-04	7.755E-06	9.849E-08	4.137E-10
T_{Ref} + 10%	7.834E-01	2.163E-01	7.644E-04	1.032E-05	1.442E-07	6.663E-10
	-2.5%	10.0%	21.0%	33.1%	46.4%	61.1%

Table 2.8: Sensitivities of the atom densities with regard to the Pu-240 capture cross-section calculated with the exact and Taylor expressions for a pure Pu-240 sample irradiated 50 days – Cadmium filter – Φ = 1.5 10^{14} n.cm^{-2}.s^{-1}

	Pu0	Pu1	Pu2	Am3	Cm4	Cm5
	Exact					
Ref	8.212E-01	1.756E-01	5.785E-04	7.167E-06	9.197E-08	3.889E-10
$\bar{\sigma}_{Pu0}^{c}$ + 10%	8.052E-01	1.913E-01	6.323E-04	7.846E-06	1.008E-07	4.265E-10
	-1.9%	9.0%	9.3%	9.5%	9.6%	9.7%
	Taylor					
Ref	8.031E-01	1.967E-01	6.317E-04	7.755E-06	9.849E-08	4.137E-10
$\bar{\sigma}_{Pu0}^{c}$ + 10%	7.834E-01	2.163E-01	6.949E-04	8.531E-06	1.083E-07	4.551E-10
	-2.5%	10.0%	10.0%	10.0%	10.0%	10.0%

Table 2.9: Sensitivities of the atom densities with regard to the Pu-241 capture cross-section calculated with the exact and Taylor expressions for a pure Pu-240 sample irradiated 50 days – Cadmium filter – Φ = 1.5 10^{14} n.cm^{-2}.s^{-1}

	Pu0	Pu1	Pu2	Am3	Cm4	Cm5
			Exact			
Ref	8.212E-01	1.756E-01	5.785E-04	7.167E-06	9.197E-08	3.889E-10
$\bar{\sigma}^c_{Pu1}$+ 10%	8.212E-01	1.755E-01	6.362E-04	7.883E-06	1.012E-07	4.278E-10
	0.00%	-0.03%	9.98%	9.98%	9.99%	10.00%
			Taylor			
Ref	8.031E-01	1.967E-01	6.317E-04	7.755E-06	9.849E-08	4.137E-10
$\bar{\sigma}^c_{Pu1}$+ 10%	8.031E-01	1.967E-01	6.949E-04	8.531E-06	1.083E-07	4.551E-10
	0.00%	0.00%	10.00%	10.00%	10.00%	10.00%

Incidentally, the last two tables also show that the sensitivities of the atom densities of isotopes A+1, A+2, A+3, etc… with regards to the capture cross section of isotope A is very close to 1. In other words, a 1% variation of the capture cross section of A induces a 1% variation of the atom densities of A+1, A+2, A+3, etc…

2.2. Determination of the time-integrated neutron flux

The time-integrated neutron flux $\int_0^T \phi(t)dt = \bar{\phi}T$ can be determined experimentally from the amount of a fission product formed during irradiation. Among the fission products, **Nd-148** has the following properties [1] to recommend it as an ideal indicator for the time-integrated neutron flux: (1) it is not volatile, does not migrate in solid fuels below their recrystallization temperature, and has no volatile precursors (2) it is nonradioactive and requires no decay corrections, (3) it has a low destruction cross-section and formation from adjacent mass chains can be corrected for, (4) it has good emission characteristics for mass analysis and (5) its fission yield is nearly the same for U-235 and Pu-239 and is essentially independent of neutron energy. In addition to Nd-148, **Cs-137** is also a good indicator of the time-integrated neutron flux.

Neglecting as a first approximation the contribution of Nd-147 captures as well as the potential time-dependence of the U-235 fission cross-section, the Nd-148 atom density in a U-235 sample after an irradiation time T is given by the following expression:

$$N_{Nd8}(T) = \gamma_{Nd8}\bar{\sigma}^f_{U5}\int_0^T N_{U5}(t)\phi(t)dt = \gamma_{Nd8}\bar{\sigma}^f_{U5}N_{U5}(0)\int_0^T e^{-\bar{\sigma}^a_{U5}\int_0^t \varphi(x)dx}\phi(t)dt \ ,$$

where γ_{Nd8} is the Nd-148 cumulative fission yield, i.e. the number of Nd-148 atoms as well as its short-lived precursors produced per fission, and the other parameters have already been defined. If $N_{U5}(t)$ is approximated by its first order development it comes that:

$$N_{Nd8}(T) \sim \gamma_{Nd8}\bar{\sigma}^f_{U5}N_{U5}(0)\int_0^T \phi(t)\left[1 - \bar{\sigma}^a_{U5}\int_0^t \phi(x)dx\right]dt$$

$$= \gamma_{Nd8}\bar{\sigma}^f_{U5}N_{U5}(0)\left\{\int_0^T \phi(t)dt - \bar{\sigma}^a_{U5}\int_0^T \phi(t)\left[\int_0^t \phi(x)dx\right]dt\right\}$$

N.B.: As long as $\bar{\sigma}^a_{U5}\int_0^t \phi(x)dx$ <0.1 the first order development agrees with the exact analytical expression at better than 0.5%. This condition is fulfilled in most practical applications. Indeed, let's consider an idealized case where a U-235 sample is irradiated in a pure Maxwellian spectrum with a (rather high) flux level of 5×10^{13} n.cm^{-2}.s^{-1}. The U-235 absorption cross-section in this spectrum being of the order of 590 barns, it will still take about 40 days before the term $\bar{\sigma}^a_{U5}\int_0^t \phi(x)dx$ reaches the value of 0.1.

After integrating by part the term $\int_0^T \phi(t) \left[\int_0^t \phi(x)dx \right] dt$ it comes that:

$$N_{Nd8}(T) \sim \gamma_{Nd8}\bar{\sigma}_{U5}^f N_{U5}(0) \int_0^T \phi(t)dt \left[1 - \frac{1}{2}\bar{\sigma}_{U5}^a \int_0^T \phi(t)dt \right] = \gamma_{Nd8}\bar{\sigma}_{U5}^f N_{U5}(0)[\bar{\phi}\,T] \left(1 - \frac{1}{2}\bar{\sigma}_{U5}^a[\bar{\phi}T] \right)$$

which can be rewritten in the form of a quadratic equation: $-\frac{\bar{\sigma}_{U5}^a}{2}[\bar{\phi}T]^2 + [\bar{\phi}T] - \frac{1}{\gamma_{Nd8}\bar{\sigma}_{U5}^f}\frac{N_{Nd8}(T)}{N_{U5}(0)} \sim 0$.
However since the measurements provide $\frac{N_{Nd8}(T)}{N_{U5}(T)}$ and not $\frac{N_{Nd8}(T)}{N_{U5}(0)}$ it is better to rewrite the above quadratic equation as:

$$-\frac{\bar{\sigma}_{U5}^a}{2}[\bar{\phi}T]^2 + \left(1 + \frac{\bar{\sigma}_{U5}^a}{\gamma_{Nd8}\bar{\sigma}_{U5}^f}\frac{N_{Nd8}(T)}{N_{U5}(T)} \right)[\bar{\phi}T] - \frac{1}{\gamma_{Nd8}\bar{\sigma}_{U5}^f}\frac{N_{Nd8}(T)}{N_{U5}(T)} \sim 0$$

The discriminant of this quadratic equation is equal to $\Delta = \left(1 + \frac{\bar{\sigma}_{U5}^a}{\gamma_{Nd8}\bar{\sigma}_{U5}^f}\frac{N_{Nd8}(T)}{N_{U5}(T)} \right)^2 -$
$2\frac{\bar{\sigma}_{U5}^a}{\gamma_{Nd8}\bar{\sigma}_{U5}^f}\frac{N_{Nd8}(T)}{N_{U5}(T)}$ and since for most practical applications $\frac{\bar{\sigma}_{U5}^a}{\gamma_{Nd8}\bar{\sigma}_{U5}^f}\frac{N_{Nd8}(T)}{N_{U5}(T)} \ll 1$ it comes that $\Delta \sim 1$. As a quadratic equation, it has two roots, however only one is consistent with the hypothesis used to derive the equation in the first place, i.e. that $\bar{\sigma}_{U5}^a\,\bar{\phi}T \leq 0.1$. It then comes that the time-integrated neutron flux in a U-235 sample can be determined from the measurement of the Nd-148 atom density relative to that of U-235 as:

$$\bar{\phi}T \sim \left[\frac{N_{Nd8}(T)}{N_{U5}(T)} \right]_m \frac{1}{\gamma_{Nd8}\bar{\sigma}_{U5}^f}$$

N.B.: The fission yield γ_{Nd8} is taken directly from existing nuclear data libraries (like ENDF/B-VII for instance) and is only very weakly problem-dependent. On the other hand, the U-235 effective one-group fission cross-section $\bar{\sigma}_{U5}^f = \frac{\int \sigma_{U5}^f(E)\omega(E)dE}{\int \omega(E)dE}$ is very strongly problem-dependent because $\omega(E)$ is the neutron spectrum in the sample ($\sigma_{U5}^f(E)$ comes from existing libraries and is only very weakly problem-dependent).

2.3. Application to the inference of neutron capture cross-sections

As an example, let's consider a very pure sample containing essentially (i.e. at least 99%) an isotope of mass number A, but also a few tenths of a percent of other isotopes present as impurities (let's say A-1, A+1, A+2 and A+3). The atom density of isotope A+1 after an irradiation time T can be expressed as:

$$N_{A+1}(T) \sim \frac{1}{2}N_{A-1}(0)\bar{\sigma}_{A-1}^c \bar{\sigma}_A^c[\bar{\phi}T]^2 + N_A(0)\bar{\sigma}_A^c[\bar{\phi}T] + N_{A+1}(0)\{1 - \tilde{\sigma}_{A+1}^a[\bar{\phi}T]\}$$

where the first and second terms correspond to the number of A+1 atoms produced by neutron captures on, respectively, the A-1 and A atoms, and the third term corresponds to what is left of the initial A+1 atoms. Since the sample is prepared so that $N_{A-1}(0) << N_A(0)$, for most practical applications the first term will be much smaller than the second one and the A+1 atom density can be expressed as:

$$N_{A+1}(T) \sim N_A(0)\bar{\sigma}_A^c[\bar{\phi}T] + N_{A+1}(0)\{1 - \tilde{\sigma}_{A+1}^a[\bar{\phi}T]\}$$

The experimental determination of the atom densities after an irradiation time T, as well as that of the time-integrated neutron flux $[\bar{\phi}T]_m$ (the subscript m stands for *measured*) allow to infer the neutron capture cross-section of isotope A as:

$$\bar{\sigma}_A^c \sim \frac{\left[\frac{N_{A+1}(T)}{N_A(0)}\right]_m - \left[\frac{N_{A+1}(0)}{N_A(0)}\right]_m \{1 - \tilde{\sigma}_{A+1}^a [\bar{\phi}T]_m\}}{[\bar{\phi}T]_m}$$

However, since at time T the measurement provides $\left[\frac{N_{A+1}(T)}{N_A(T)}\right]_m \equiv [R_{A+1}(T)]_m$ and not $\left[\frac{N_{A+1}(T)}{N_A(0)}\right]_m$, it comes that:

$$\bar{\sigma}_A^c \sim \frac{\left[\frac{N_{A+1}(T)}{N_A(T)}\right]_m \{1 - \tilde{\sigma}_A^a [\bar{\phi}T]_m\} - \left[\frac{N_{A+1}(0)}{N_A(0)}\right]_m \{1 - \tilde{\sigma}_{A+1}^a [\bar{\phi}T]_m\}}{[\bar{\phi}T]_m}$$
$$\equiv \frac{[R_{A+1}(T)]_m\{1 - \tilde{\sigma}_A^a[\bar{\phi}T]_m\} - [R_{A+1}(0)]_m\{1 - \tilde{\sigma}_{A+1}^a[\bar{\phi}T]_m\}}{[\bar{\phi}T]_m}$$

and since $\tilde{\sigma}_A^a = \bar{\sigma}_A^c + \bar{\sigma}_A^f + \frac{\lambda_A}{\bar{\phi}}$ it finally comes that:

$$\bar{\sigma}_A^c \sim \frac{[R_{A+1}(T)]_m\{1 - \tilde{\sigma}_A^f[\bar{\phi}T]_m - \lambda_A[T]_m\} - [R_{A+1}(0)]_m\{1 - \tilde{\sigma}_{A+1}^a[\bar{\phi}T]_m\}}{[\bar{\phi}T]_m(1 + [R_{A+1}(T)]_m)}$$

If the terms {1-…} and {1+…} are approximated by 1 (which is generally a good approximation when $\bar{\phi}T$ is not too large, i.e. as long as it is smaller than about 10^{21} n.cm^{-2}), the expression simplifies as:

$$\bar{\sigma}_A^c \sim \frac{[R_{A+1}(T)]_m - [R_{A+1}(0)]_m}{[\bar{\phi}T]_m}$$

N.B.: If the capture reaction rate on the isotope A-2 is negligible compared to the (*n,2n*) reaction rate on the isotope A, then the (*n,2n*) cross-section of isotope A can be inferred using the same expression as for the capture cross-section where R_{A+1} is simply replaced by R_{A-1} :

$$\bar{\sigma}_A^{n,2n} \sim \frac{[R_{A-1}(T)]_m\{1 - \tilde{\sigma}_A^f[\bar{\phi}T]_m - \lambda_A[T]_m\} - [R_{A-1}(0)]_m\{1 - \tilde{\sigma}_{A-1}^a[\bar{\phi}T]_m\}}{[\bar{\phi}T]_m(1 + [R_{A-1}(T)]_m)} \sim \frac{[R_{A-1}(T)]_m - [R_{A-1}(0)]_m}{[\bar{\phi}T]_m}$$

However, contrary to capture reactions which occur at all neutron energies, the (*n,2n*) reactions occur only for neutrons with energies higher than about 5 MeV (Figure 2.2). Consequently the effective (*n,2n*) cross-sections can be thousands of times smaller than the effective capture cross-sections and care should be exercised before neglecting the capture reaction rate on the isotope A-2 even when $N_{A-2}(0) \ll N_A(0)$.
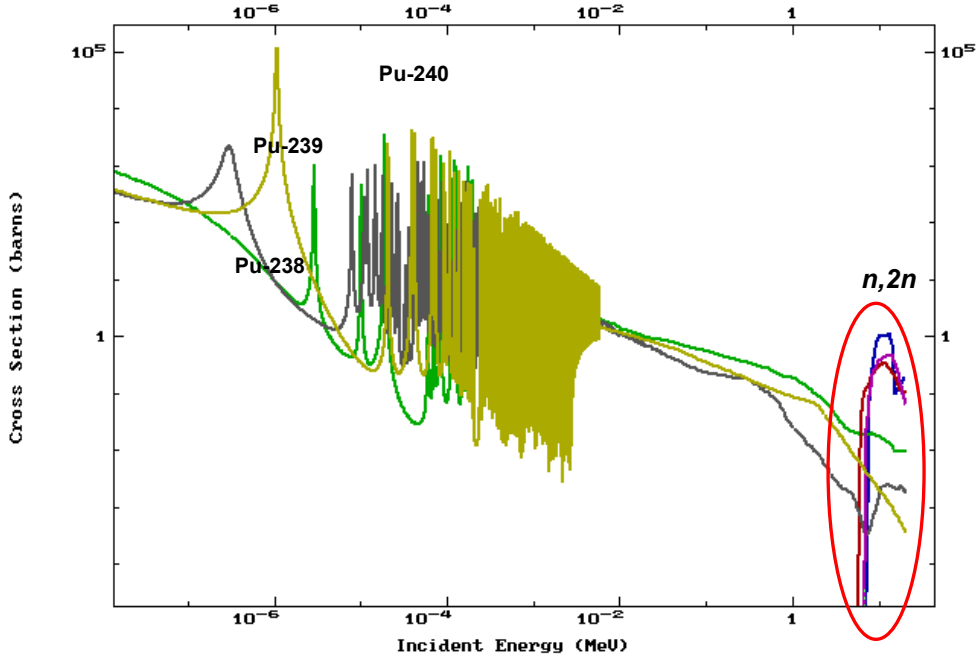
Figure 2.2. Neutron capture and (*n,2n*) cross-sections of Pu-238, Pu-239 and Pu-240 as a function of the incident neutron energy, and taken from the ENDF/B-VII.0 library.

The $N_{A+2}(T)$ atom density is given by:

$$N_{A+2}(T) \sim \frac{1}{2} N_A(0)\bar{\sigma}_A^c \bar{\sigma}_{A+1}^c [\bar{\phi}T]^2 + N_{A+1}(0)\bar{\sigma}_{A+1}^c [\bar{\phi}T] + N_{A+2}(0)\{1 - \tilde{\sigma}_{A+2}^a [\bar{\phi}T]\}$$

and the capture cross-section can be inferred as: $\bar{\sigma}_{A+1}^c \sim \dfrac{\left[\frac{N_{A+2}(T)}{N_A(0)}\right]_m - \left[\frac{N_{A+2}(0)}{N_A(0)}\right]_m \{1 - \tilde{\sigma}_{A+2}^a [\bar{\phi}T]_m\}}{\frac{1}{2}\bar{\sigma}_A^c [\bar{\phi}T]_m^2 + \left[\frac{N_{A+1}(0)}{N_A(0)}\right]_m [\bar{\phi}T]_m}$.

However, since at time T the measurement provides $\left[\frac{N_{A+2}(T)}{N_A(T)}\right]_m \equiv [R_{A+2}(T)]_m$ and not $\left[\frac{N_{A+2}(T)}{N_A(0)}\right]_m$, it comes that:

$$\bar{\sigma}_{A+1}^c \sim \frac{[R_{A+2}(T)]_m \{1 - \tilde{\sigma}_A^f [\bar{\phi}T]_m - \lambda_A[T]_m\} - [R_{A+2}(0)]_m \{1 - \tilde{\sigma}_{A+2}^a [\bar{\phi}T]_m\}}{\left(\frac{1}{2}\bar{\sigma}_A^c [\bar{\phi}T]_m^2 + [R_{A+1}(0)]_m [\bar{\phi}T]_m\right)(1 + [R_{A+2}(T)]_m)}$$

Substituting $\bar{\sigma}_A^c$ by its expression as a function of the measured quantities leads finally to:

$$\bar{\sigma}_{A+1}^c \sim \frac{[R_{A+2}(T)]_m \{1 - \tilde{\sigma}_A^f [\bar{\phi}T]_m - \lambda_A[T]_m\} - [R_{A+2}(0)]_m \{1 - \tilde{\sigma}_{A+2}^a [\bar{\phi}T]_m\}}{\left(\frac{1}{2}\frac{[R_{A+1}(T)]_m \{1 - \tilde{\sigma}_A^f [\bar{\phi}T]_m - \lambda_A[T]_m\} - [R_{A+1}(0)]_m \{1 - \tilde{\sigma}_{A+1}^a [\bar{\phi}T]_m\}}{(1 + [R_{A+1}(T)]_m)} [\bar{\phi}T]_m + [R_{A+1}(0)]_m [\bar{\phi}T]_m\right)(1 + [R_{A+2}(T)]_m)}$$

If, as previously, the terms {1-…} and {1+…} are approximated by 1, the expression simplifies as:

$$\bar{\sigma}_{A+1}^c \sim 2 \frac{[R_{A+2}(T)]_m - [R_{A+2}(0)]_m}{([R_{A+1}(T)]_m + [R_{A+1}(0)]_m)[\bar{\phi}T]_m}$$

and if, furthermore, the initial A+1 and A+2 atom densities are negligible in comparison to those at time T (this is very sample-dependent and can be a very bad approximation when $\bar{\phi}T$ is not too large), the A+1 capture cross-section is simply equal to:

$$\bar{\sigma}^c_{A+1} \sim 2 \frac{[R_{A+2}(T)]_m}{[R_{A+1}(T)]_m[\bar{\phi}T]_m}$$

Finally, the $N_{A+3}(T)$ atom density is given by:

$$N_{A+3}(T) \sim \frac{1}{6}N_A(0)\bar{\sigma}^c_A\bar{\sigma}^c_{A+1}\bar{\sigma}^c_{A+2}[\bar{\phi}T]^3 + \frac{1}{2}N_{A+1}(0)\bar{\sigma}^c_{A+1}\bar{\sigma}^c_{A+2}[\bar{\phi}T]^2 + N_{A+2}(0)\bar{\sigma}^c_{A+2}[\bar{\phi}T]$$
$$+ N_{A+3}(0)\{1 - \tilde{\sigma}^a_{A+3}[\bar{\phi}T]\}$$

and the cross-section by:

$$\bar{\sigma}^c_{A+2} \sim \frac{[R_{A+3}(T)]_m\{1 - \tilde{\sigma}^f_A[\bar{\phi}T]_m - \lambda_A[T]_m\} - [R_{A+3}(0)]_m\{1 - \tilde{\sigma}^a_{A+3}[\bar{\phi}T]_m\}}{\left(\frac{1}{6}\bar{\sigma}^c_A\bar{\sigma}^c_{A+1}[\bar{\phi}T]^3_m + \frac{1}{2}[R_{A+1}(0)]_m\bar{\sigma}^c_{A+1}[\bar{\phi}T]^2_m + [R_{A+2}(0)]_m[\bar{\phi}T]_m\right)(1 + [R_{A+3}(T)]_m)}$$

Substituting $\bar{\sigma}^c_A$ and $\bar{\sigma}^c_{A+1}$ by their expressions as a function of the measured quantities leads to a somewhat cumbersome expression and is not reproduced here. However, if, as previously, the terms {1-…} and {1+…} are approximated by 1, the expression simplifies as:

$$\bar{\sigma}^c_{A+2} \sim 3 \frac{([R_{A+3}(T)]_m - [R_{A+3}(0)]_m)([R_{A+1}(T)]_m + [R_{A+1}(0)]_m)}{[[R_{A+1}(T)]_m([R_{A+2}(T)]_m + 2[R_{A+2}(0)]_m) + [R_{A+1}(0)]_m(2[R_{A+2}(T)]_m + [R_{A+2}(0)]_m)][\bar{\phi}T]_m}$$

and if, furthermore, the initial A+2 and A+3 atom densities are negligible in comparison to those at time T, the A+2 capture cross-section is simply equal to:

$$\bar{\sigma}^c_{A+2} \sim 3 \frac{[R_{A+3}(T)]_m}{[R_{A+2}(T)]_m[\bar{\phi}T]_m}$$

Similarly, if all the initial atom densities are negligible in comparison to those at time T, the A+n capture cross-section is simply equal to:

$$\bar{\sigma}^c_{A+n} \sim (n+1) \frac{[R_{A+n+1}(T)]_m}{[R_{A+n}(T)]_m[\bar{\phi}T]_m}$$

3. UNCERTAINTY QUANTIFICATION – DERIVATION OF THE EXPRESSIONS RELATIVE TO THE INFERRED CAPTURE CROSS-SECTIONS AND TIME-INTEGRATED FLUX

As shown above, the inferred capture cross-sections are all expressed as ratios like $\bar{\sigma}^c \sim \frac{X}{Y}$. Using the recommended, and widely accepted, laws of propagation of uncertainties (see for example [**2**] and [**3**]), the relative uncertainty of the inferred cross-sections can be expressed as a function of the relative uncertainties of X and Y as:

$$\frac{u(\bar{\sigma}^c)}{\bar{\sigma}^c} = \sqrt{\left(\frac{u(X)}{X}\right)^2 + \left(\frac{u(Y)}{Y}\right)^2 - 2r_{XY}\left(\frac{u(X)}{X}\right)\left(\frac{u(Y)}{Y}\right)}$$

where $r_{XY} = 0$ if X and Y are not correlated, i.e. if they are independent, and $-1 \le r_{XY} \le +1$ otherwise.

Without specific information about the correlations, and as a first guess, X and Y will be considered independent so that the relative uncertainty of the inferred cross-sections can be expressed as:

$$\frac{u(\bar{\sigma}^c)}{\bar{\sigma}^c} = \sqrt{\left(\frac{u(X)}{X}\right)^2 + \left(\frac{u(Y)}{Y}\right)^2}$$

As examples, let's consider the uncertainty of the inferred A and A+1 capture cross-sections. Since the inferred capture cross-section of A is expressed as (see previous chapter)

$$\bar{\sigma}_A^c \sim \frac{[R_{A+1}(T)]_m\{1 - \tilde{\sigma}_A^f[\bar{\phi}T]_m - \lambda_A[T]_m\} - [R_{A+1}(0)]_m\{1 - \tilde{\sigma}_{A+1}^a[\bar{\phi}T]_m\}}{[\bar{\phi}T]_m(1 + [R_{A+1}(T)]_m)}$$

It then comes that: $X_A = [R_{A+1}(T)]_m\{1 - \tilde{\sigma}_A^f[\bar{\phi}T]_m - \lambda_A[T]_m\} - [R_{A+1}(0)]_m\{1 - \tilde{\sigma}_{A+1}^a[\bar{\phi}T]_m\}$ and $Y_A = [\bar{\phi}T]_m(1 + [R_{A+1}(T)]_m)$.

The relative uncertainty of the numerator is then expressed as:

$$\left(\frac{u(X_A)}{X_A}\right) = \frac{\sqrt{\begin{array}{c}\{u([R_{A+1}(T)]_m)\}^2\{1 - \bar{\sigma}_A^f[\bar{\phi}T]_m - \lambda_A[T]_m\}^2 + \{[R_{A+1}(T)]_m\}^2\{\bar{\sigma}_A^f[\bar{\phi}T]_m\}^2\left\{\left[\frac{u(\bar{\sigma}_A^f)}{\bar{\sigma}_A^f}\right]^2 + \left[\frac{u([\bar{\phi}T]_m)}{[\bar{\phi}T]_m}\right]^2\right\} + \\ \{u([R_{A+1}(0)]_m)\}^2\{1 - \tilde{\sigma}_{A+1}^a[\bar{\phi}T]_m\}^2 + \{[R_{A+1}(0)]_m\}^2\{\tilde{\sigma}_{A+1}^a[\bar{\phi}T]_m\}^2\left\{\left[\frac{u(\tilde{\sigma}_{A+1}^a)}{\tilde{\sigma}_{A+1}^a}\right]^2 + \left[\frac{u([\bar{\phi}T]_m)}{[\bar{\phi}T]_m}\right]^2\right\}\end{array}}}{[R_{A+1}(T)]_m\{1 - \bar{\sigma}_A^f[\bar{\phi}T]_m - \lambda_A[T]_m\} - [R_{A+1}(0)]_m\{1 - \tilde{\sigma}_{A+1}^a[\bar{\phi}T]_m\}}$$

where the uncertainty of the natural decay term $\lambda_A[T]_m$ has been neglected because for most practical applications its uncertainty is much smaller than that of the other terms. Furthermore, as long as $\bar{\phi}T$ is not too large, i.e. as long as it is smaller than about 10^{21} n.cm^{-2}, then for most cases $\bar{\sigma}_A^f[\bar{\phi}T]_m \ll 1$ and $\tilde{\sigma}_{A+1}^a[\bar{\phi}T]_m \ll 1$ and consequently this expression can be approximated as:

$$\left(\frac{u(X_A)}{X_A}\right) \cong \frac{\sqrt{\{u([R_{A+1}(T)]_m)\}^2\{1 - \bar{\sigma}_A^f[\bar{\phi}T]_m - \lambda_A[T]_m\}^2 + \{u([R_{A+1}(0)]_m)\}^2\{1 - \tilde{\sigma}_{A+1}^a[\bar{\phi}T]_m\}^2}}{[R_{A+1}(T)]_m\{1 - \bar{\sigma}_A^f[\bar{\phi}T]_m - \lambda_A[T]_m\} - [R_{A+1}(0)]_m\{1 - \tilde{\sigma}_{A+1}^a[\bar{\phi}T]_m\}}$$

or, simplifying further as

$$\left(\frac{u(X_A)}{X_A}\right) \cong \frac{\sqrt{\{u([R_{A+1}(T)]_m)\}^2 + \{u([R_{A+1}(0)]_m)\}^2}}{[R_{A+1}(T)]_m - [R_{A+1}(0)]_m}$$

The relative uncertainty of the denominator is simply expressed as: $\frac{u(Y_A)}{Y_A} = \frac{u([\bar{\phi}T]_m)}{[\bar{\phi}T]_m}$ since the uncertainty of the term $(1 + [R_{A+1}(T)]_m)$ is negligible because, for most practical applications, $[R_{A+1}(T)]_m \ll 1$. Hence, for most practical applications the relative uncertainty of $\bar{\sigma}_A^c$ can be estimated as:

$$\left(\frac{u(\bar{\sigma}_A^c)}{\bar{\sigma}_A^c}\right) \sim \sqrt{\left(\frac{\sqrt{\{u([R_{A+1}(T)]_m)\}^2 + \{u([R_{A+1}(0)]_m)\}^2}}{[R_{A+1}(T)]_m - [R_{A+1}(0)]_m}\right)^2 + \left(\frac{u([\bar{\phi}T]_m)}{[\bar{\phi}T]_m}\right)^2}$$

Similarly, the expression for the inferred capture cross-section of A+1 being

$$\bar{\sigma}_{A+1}^c \sim 2 \frac{[R_{A+2}(T)]_{m-}[R_{A+2}(0)]_m}{([R_{A+1}(T)]_m + [R_{A+1}(0)]_m)[\bar{\phi}T]_m}$$

it then comes that:

$$\left(\frac{u(\bar{\sigma}_{A+1}^c)}{\bar{\sigma}_{A+1}^c}\right) \sim \sqrt{\left(\frac{\sqrt{\{u([R_{A+2}(T)]_m)\}^2 + \{u([R_{A+2}(0)]_m)\}^2}}{[R_{A+2}(T)]_m - [R_{A+2}(0)]_m}\right)^2 + \left(\frac{\sqrt{\{u([R_{A+1}(T)]_m)\}^2 + \{u([R_{A+1}(0)]_m)\}^2}}{[R_{A+1}(T)]_m + [R_{A+1}(0)]_m}\right)^2 + \left(\frac{u([\bar{\phi}T]_m)}{[\bar{\phi}T]_m}\right)^2}$$

Similar expressions can be derived for the A+2, A+3... capture cross-sections, but are not reproduced here because they become quickly cumbersome. They can be used to determine the uncertainty of the inferred cross-sections given the uncertainty of the measurement of the nuclide densities and that of the measurement of the time-integrated flux. Inversely, they can be used as well to determine the experimental uncertainties that are necessary to obtain the inferred cross-sections with a given target uncertainty. This will be presented later in this document.

The uncertainty of the time-integrated flux is obtained the same way. Indeed, since the time-integrated flux in a U-235 sample is given by the expression (see section 2.2):

$$\bar{\phi}T \sim \left[\frac{N_{Nd8}(T)}{N_{U5}(T)}\right]_m \frac{1}{\gamma_{Nd8}\bar{\sigma}_{U5}^f}$$

it then comes that:

$$\frac{u([\bar{\phi}T]_m)}{[\bar{\phi}T]_m} \sim \sqrt{\left(\frac{u([R_{Nd8}(T)]_m)}{[R_{Nd8}(T)]_m}\right)^2 + \left(\frac{u(\gamma_{Nd8})}{\gamma_{Nd8}}\right)^2 + \left(\frac{u(\bar{\sigma}_{U5}^f)}{\bar{\sigma}_{U5}^f}\right)^2} \quad \text{with } [R_{Nd8}(T)]_m \equiv \left[\frac{N_{Nd8}(T)}{N_{U5}(T)}\right]_m$$

The uncertainty of the Nd-148 fission yield (γ_{Nd8}) and that of the U-235 fission cross-section $\left(\bar{\sigma}_{U5}^f(E)\right)$ are only of the order of half a percent. However, since the U-235 effective one-group fission cross-section is calculated as $\bar{\sigma}_{U5}^f = \frac{\int \bar{\sigma}_{U5}^f(E)\omega(E)dE}{\int \omega(E)dE}$, where $\omega(E)$ is the neutron spectrum in the sample, the term $\frac{u(\bar{\sigma}_{U5}^f)}{\bar{\sigma}_{U5}^f}$ should then take into account the uncertainty of the basic nuclear data $\bar{\sigma}_{U5}^f(E)$ as well as that of the calculated neutron spectrum $\omega(E)$. The latter comes from the calculations themselves (e.g. statistical uncertainty if $\omega(E)$ is calculated with a Monte-Carlo code) and from the uncertainties related to the conditions of the measurement that could potentially impact $\omega(E)$.

4. SAMPLES IRRADIATION IN THE ADVANCED TEST REACTOR

The Advanced Test Reactor (ATR) is located at the ATR Complex on the INL site and has been operating continuously since 1967. The primary mission of this versatile facility was initially to serve the U.S. Navy in the development and refinement of nuclear propulsion systems, however, in recent years the ATR has been used for a wider variety of government and privately sponsored research. DOE's designation of the ATR as a National Scientific User Facility enables DOE to facilitate research that would not have been feasible for many researchers and allows for fuller utilization of the ATR as a government asset.

The ATR design exploits a unique serpentine core configuration (Figure 4.1) that offers a large number of test positions. It has large test volumes in high-flux areas designed to permit simulation of long neutron irradiation exposures in a short period of time. The maximum thermal power rating is 250 MWth with a maximum unperturbed thermal neutron flux of 10^{15} n.cm^{-2}.s^{-1}. Since most contemporary experimental objectives generally do not require the limits of its operational capability, the ATR typically operates at much lower power levels. Occasionally, some lobes of the reactor are operated at higher powers that generate higher neutron flux.
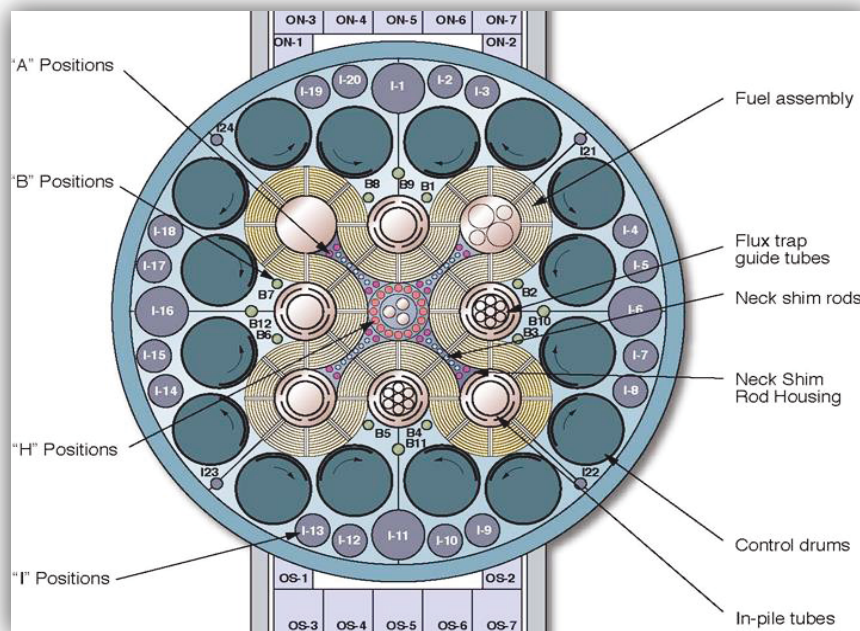
Figure 4.1. ATR core cross section.

The ATR is cooled by pressurized (2.5 MPa) water that enters the reactor vessel bottom at an average temperature of 52°C, flows up outside cylindrical tanks that support and contain the core, passes through concentric thermal shields into the open upper part of the vessel, then flows down through the core to a flow distribution tank below the core. When the reactor is operating at full power, the primary coolant exits the vessel at a temperature of 71°C.

The ATR operates in cycles that typically range in duration from 6 to 8 weeks of operating time, preceded by an outage that is typically one to two weeks in duration. Experiments may be inserted or removed only during the scheduled shutdowns (outages) that occur between the operating cycles. In addition to the regular 6 to 8 week cycles, high power cycles identified as Powered Axial Locator Mechanism (PALM) are occasionally scheduled for short durations. These cycles typically run from 7 to 14 days with lobe powers as high as 50 MW.

The unique design of ATR control devices permits large power variations among its nine flux traps using a combination of control cylinders (drums) and neck shim rods. The beryllium control cylinders contain hafnium plates that can be rotated toward and away from the core, and hafnium shim rods, which withdraw vertically, can be individually inserted or withdrawn for minor power adjustments. Within bounds,

the power level in each corner lobe of the reactor can be controlled independently to allow for different power and flux levels in the four corner lobes during the same operating cycle. More information on the ATR and its associated post irradiation capabilities can be found for example in Ref. [**4**].

The list of actinides that were irradiated is the following: Th-232, U-233, U-235, U-236, U-238, Np-237, Pu-239, Pu-240, Pu-242, Pu-244, Am-241, Am-243, Cm-244 and Cm-248. The list of fission products is the following: Sm-149, Eu-153, Cs-133, Rh-103, Ru-101, Nd-143, Nd-145 and Pd-105. A total of 21 capsules containing between about 0.5 and 3 mg of each sample are piled on top of each other and are located in the large B9 and B11 positions (see Figure 4.1).

Four capsules containing U-235 wires positioned between the capsules containing the samples have also been used to determine the neutron fluence experimentally. As it was shown in section 2, the determination of the fluence is crucial for this kind of experiment. It will be determined experimentally from the amount of Nd-148 and Cs-137 formed during irradiation.

In order to obtain effective neutron capture cross sections corresponding to different neutron spectra, three sets of actinide samples have been irradiated: the first one is filtered with **cadmium** and the other two are filtered with **enriched boron** of different thicknesses (5 mm and 10 mm) as shown on Figure 4.2.

Sm149	1
Np237	2
flux wires	3
Am243	4
U233	5
U235	6
Cm248	7
Pu242	8
Pu244	9
flux wires	10
Pu240	11
Th232	12
Am241	13
Np237	14
Pu244	15
Cm248	16
flux wires	17
U238	18
Am243	19
Pu239	20
U236	21
Pu242	22
flux wires	23
Am241	24
Eu-Cs-Rh	25

(a)

(b)

(c)

(d)

(e)
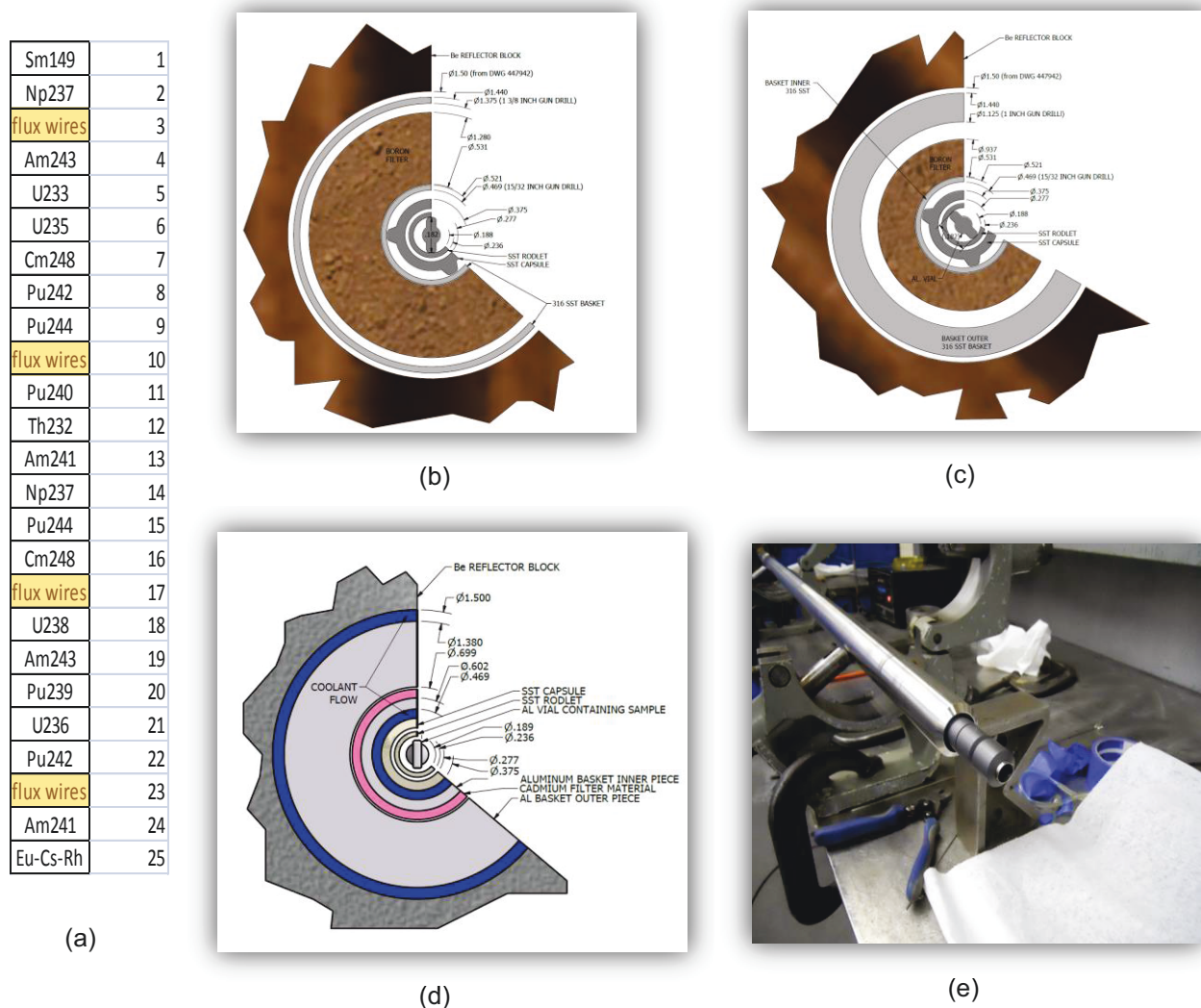
Figure 4.2. Boron-filtered sample loading plan (a), 10-mm-boron filter (b), 5-mm-boron filter (c), cadmium filter (d) and photo of boron filter (e)

The neutron capture reactions of B-10 and Cd-113 have large cross-sections and strongly impact the neutron spectrum (Figure 4.3) allowing the samples to be irradiated in epithermal and fast neutron

spectra whereas the unfiltered neutron spectrum is largely thermal. The total flux levels in the samples are, respectively, about 2×10^{14} n.cm^{-2}.s^{-1} and 10^{14} n.cm^{-2}.s^{-1} with the cadmium filter and the boron filters.

The cadmium-filtered and the 5-mm-boron-filtered irradiations were completed in January 2013 after, respectively, 55 days and 110 days in the reactor. The last irradiation with the 10-mm boron filter was completed in January 2014 after approximately 110 days in the reactor.
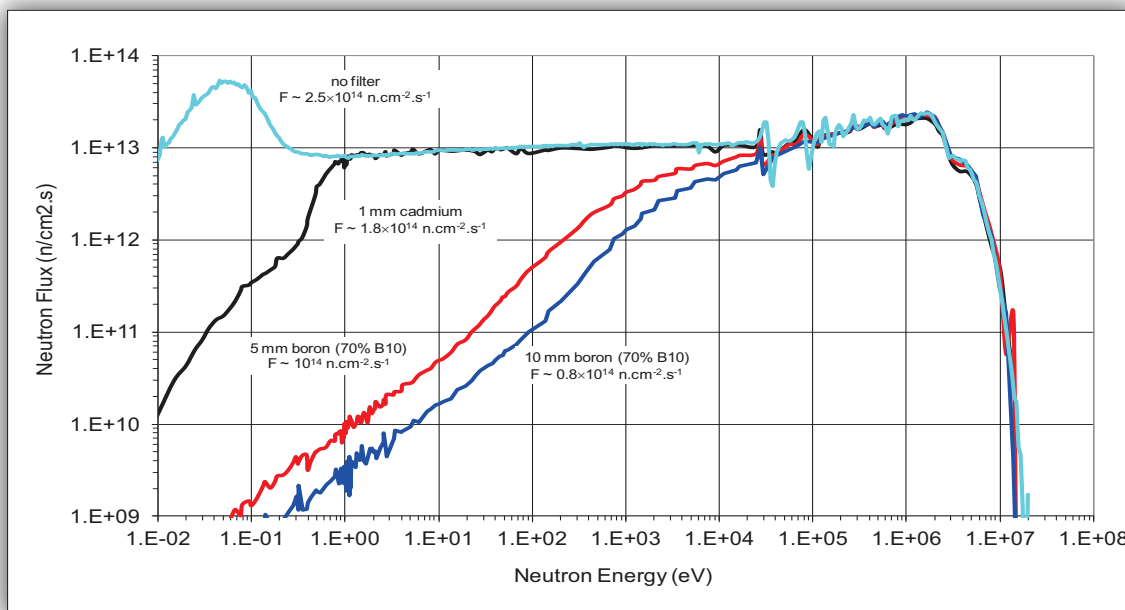
Figure 4.3. Neutron flux in the samples with boron and cadmium filters as calculated with MCNP

5. EXPERIMENTAL DETERMINATION OF THE ATOM DENSITIES OF THE TRANSMUTATION PRODUCTS WITH MULTI-COLLECTOR INDUCTIVELY COUPLED PLASMA MASS SPECTROMETER (MC-ICP-MS)

5.1. Experimental protocol

After a cool-down time in the ATR canal, the baskets containing the irradiated samples were transported to the hot cells of the Hot Fuel Examination Facility (HFEF) located at the Materials and Fuels Complex (MFC) where they were dismantled. INL utilizes HFEF capabilities in researching radioactive materials development and characterization. The vials containing the samples were then sent to the nearby Analytical Laboratory for further analyses.
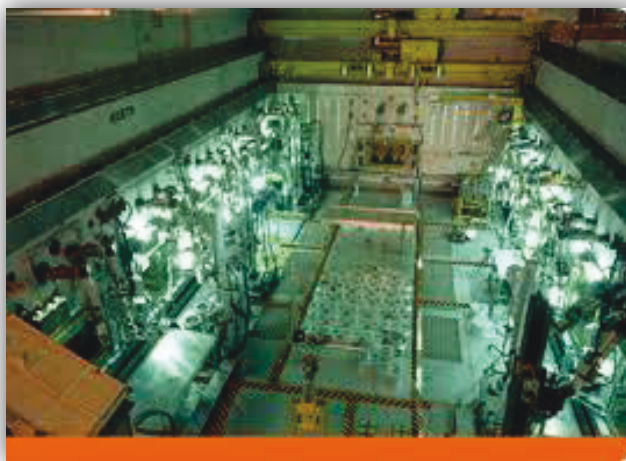
Figure 5.1. ATR canal (left) and HFEF hot cell (right)

The stable fission products and actinide targets were received in the Analytical Laboratory Hot Cells (ALHC), and transferred into a laboratory glovebox for dissolution. The Analytical Laboratory has six shielded hot cells for receiving and analyzing highly radioactive materials. The hot cells are made of two feet thick, high-density concrete, with leaded glass shielding windows. The cells underwent a safety upgrade in 1993. A pneumatic transfer system brings samples to the hot cells from other facilities or moves finished samples to a waste cask for disposal. The hot cells include:

<u>Cell 1</u>: Sample Receiving – Samples are received using a pneumatic system
<u>Cell 2</u>: Sample Dissolution – Samples or small portions of samples are dissolved
<u>Cell 3</u>: Sample Storage – A rotating sample rack is used for sample storage
<u>Cell 4</u>: Gamma Spectroscopy – Some samples are too radioactive to be taken to the counting lab. Therefore, a gamma spectrometer is used to count hot samples inside the hot cell. For fuel pins, the cell contains a micro gamma scanner, which only measures a small area of the sample at a time, while the sample is moved very slowly past, at a rate of approximately 0.5 millimeters per second.
<u>Cell 5</u>: Used for Multi-Programmatic R&D Instrumentation
<u>Cell 6</u>: Transfer Tube to Lead-Shielded ICP-AES (inductively coupled plasma atomic emission spectrometry) glovebox. Once the samples have been prepared in the hot cell, they can be transferred to the ICP-AES glovebox without removal from the hot cell.

A chain-driven cart moves samples from one cell to the next, and the manipulators allow staff to work with the samples without danger of exposure.

Figure 5.2. Analytical Laboratory hot cells (left) and gloveboxes (right)

The target isotope (0.5-3 mg) was left in the sealed aluminum capsule (37.5 mg) for the dissolution process. The sample was placed in a Teflon beaker with 3 mL 4$\underline{M}$ HCl, and allowed to react at ambient temperature with the aluminum capsule for ~20 minutes, or until reaction ceased. The sample was heated to completely dissolve the aluminum capsule in ~10 minutes at low heat. The remaining target (oxide or nitrate) residue was treated by addition of aqua regia (2 mL 12$\underline{M}$ HCl + 1 mL 16$\underline{M}$ HNO$_3$) and heating at medium to high heat. Multiple treatments with aqua regia were required in order to dissolve the target residue. Hydrofluoric acid (~0.4 mL 24$\underline{M}$ HF) was added during the aqua regia treatment, in order to complex free aluminum and act as a dissolution catalyst. Once the target residue was dissolved, boric acid (2 mL 4% H$_3$BO$_4$) was added to complex free fluoride and to dissolve any actinide or rare earth fluorides that had formed. The sample was heated to ensure complete dissolution of fluorides and reduce volume. The sample was quantitatively transferred to a 5 mL dissolver vial with dilute HNO$_3$, and a stable dissolver weight obtained.

Several problems were observed during the dissolution process. The higher fluence samples were typically harder to dissolve, and required at least 1 ½ to 2 days of acid treatments. The aluminum capsule had an insoluble gray-dark gray skin that was not dissolved by the initial HCl treatment, and required additional aqua regia treatments to affect dissolution. In general, the nitrate targets were harder to dissolve than the oxide targets. The insoluble aluminum skins were assumed to be the formation of the alpha aluminum oxide on the surface of the irradiated capsule. The initial insoluble residue found in the dissolution of the nitrate targets was believed to be the formation of actinide carbides from the ^{14}N(n,p)^{14}C

reaction during irradiation. Some samples were a challenge to dissolve, taking up to 2 days of treatment, in order to obtain a clear dissolver solution.

The flux wires were received in the Analytical Laboratory Hot Cells (ALHC), and transferred into a laboratory hood. After initial gamma spectroscopy was performed on the solid wires (Co, Ni, Ti, Cu, Fe, and U), the uranium flux wires were dissolved. The uranium flux wire weight was obtained (~15 mg) prior to dissolution. The flux wire was placed in a Teflon beaker, and added a mixture of 2 mL 12$\underline{M}$ HCl + 1 mL 16$\underline{M}$ HNO3 + 1 mL 2$\underline{M}$ HF dropwise to react with the sample at ambient temperature. After 90 minutes, the sample was dissolved, and heated to reduce volume. Nitric acid (1 mL 16$\underline{M}$ HNO$_3$) was then added, to react with and remove the chloride (HCl) from the sample matrix, with additional heating to reduce volume. Boric acid (1 mL 4% H$_3$BO$_4$) was then added to remove all free fluoride and to dissolve any uranium fluoride (UF$_4$) formed during the dissolution. After additional heating to reduce volume, the dissolver solution was quantitatively transferred to a poly bottle with 8$\underline{M}$ HNO$_3$, and a stable dissolver weight was obtained (~20 mL volume). The dissolved flux wire solutions were submitted for ICP-MS measurement of uranium (and other selected isotopes) and gamma spectroscopy. There was no problem noted during the flux wire dissolutions.

A powerful new research tool, the MC-ICP-MS was brought online in INL's Analytical Lab in April 2013. It greatly increases the speed and precision of the lab's ability to complete isotopic analysis on material samples. The MC-ICP-MS represents a leap above the DOE and industry standard for accurate measurements of isotopic ratios, which relied on a technology in place since the mid-1980s, called a thermal ionization mass spectrometer, or TIMS. TIMS has typically been used only for uranium and plutonium determinations, with turnaround times of about two weeks for a given sample. Note that MC-ICP-MS does not discriminate isotopes having the same mass number. If this is necessary, a chemical separation will be required prior to the MC-ICP-MS measurements.

Figure 5.2. INL's Multi-Collector Inductively Coupled Plasma Mass Spectrometer (MC-ICP-MS)

For analysis by MC-ICP-MS, the dissolved samples were diluted to acceptable concentrations that are dictated by both administrative control requirements and instrument limitations. Samples were analyzed from lowest m/z to highest m/z to eliminate cross-contamination within the instrument during analysis. Standard operational procedure for the MC-ICP-MS includes daily instrument signal optimization, detector gain calibration (both faraday cups and ion counters) and mass bias determination. The instrumental mass bias is measured using either 235/238 ratio in NBL CRM U500 for uranium samples or 239/242 ratio in NBL CRM 128 for plutonium samples. Due to unavailability of certified Th, Np, Cm, & Am isotopic standards, mass bias for these samples were determined using either U500 or CRM 128 NBL isotopic standards. Cup configurations were such that the A+1 isotope signal is measured using an ion counter (electron multiplier) for added sensitivity. Instrument mass biases were calculated using either the linear or exponential equation.

$$MB_{Linear} = \frac{\left(\frac{\left(TR_{\frac{A}{B}} / MR_{\frac{A}{B}}\right)-1}{}\right)}{(A-B)} \quad ; \quad MBCF_{A/B} = 1 + (A-B)MB_{Linear}$$

$$MB_{Exp} = \frac{\log\left(TR_{\frac{A}{B}} / MR_{\frac{A}{B}}\right)}{\log(A/B)} \quad ; \quad MBCF_{A/B} = (A/B)^{MB_{Exp}}$$

Where:

MB_{Linear} = Linear mass bias

MB_{Exp} = Exponential mass bias

$MBCF_{A/B}$ = Mass bias correction factor for isotope ratio A/B

$TR_{\frac{A}{B}}$ = True (certified) ratio of isotope A to isotope B

$MR_{\frac{A}{B}}$ = Measured ratio of isotope A to isotope B

A = atomic mass of isotope A

B = atomic mass of isotope B

The reported uncertainty for each measured ratio was determined using GUM (Guide to the Expression of Uncertainty Measurements) with *k*=2.

5.2 Results – Actinides and fission products samples

The MC-ICP-MS measurement campaign was very successful with about 65 samples (initial + irradiated) characterized in a relatively short period of time. All the isotopic ratios of interest have an associated 2-sigma uncertainty comprised between 0.5% and 1% which was what was requested.

As of today, the MC-ICP-MS analyses have been completed for the samples irradiated with the 5-mm-boron filter and with the cadmium filter. The isotopic ratios in the pre-irradiated and irradiated samples together with their associated 2-sigma uncertainties are presented in the table below. The MC-ICP-MS analyses for the samples irradiated with the 10-mm-boron filter will be completed in 2015.

This table shows that the samples used were of excellent purity, i.e. they are all at least 99% pure. After irradiation, less than 1% of the initial material was transmuted when the 5-mm-boron filter was used whereas up to 25% was transmuted when the cadmium filter was used (see Pu-240-3 sample). This was expected as the capture reaction rates in the resonance region seen by the cadmium-filtered samples are higher than those in the faster neutron region seen by the 5-mm-boron-filtered samples.

Table 5.1: Characterization of the irradiated and non-irradiated samples with MC-ICP-MS

Th-232-2

	m/z	96589	Pre-irradiated
		Ratio ± *U*	Ratio ± *U*
Th232	231/232	(3.23 ± 0.41) E-04	< 7.90E-08
	232/232	---	---
	233/232	(6.562 ± 0.032) E-03	< 1.00E-08
	234/232	(2.1 ± 1.2) E-03	< 7.30E-07
	235/232	(5.86 ± 0.39) E-02	(3.76 ± 0.82) E-06
	236/232	< 1.0 E-03	(1.32 ± 0.49) E-06

Th-232-1

	m/z	96590	Pre-irradiated
		Ratio ± *U*	Ratio ± *U*
Th232	231/232	(7.85 ± 0.71) E-06	< 7.90E-08
	232/232	---	---
	233/232	(9.711 ± 0.052) E-04	< 1.00E-08
	234/232	< 9.3 E-06	< 7.30E-07
	235/232	(1.538 ± 0.074) E-04	(3.76 ± 0.82) E-06

	236/232	< 5.6 E-06	(1.32 ± 0.49) E-06

U-233-1

	Ratio	96596	Pre-irradiated
		Ratio ± *U*	Ratio ± *U*
U233	233/233	---	---
	234/233	(2.385 ± 0.011) E-03	(1.7383 ± .0015) E-03
	235/233	(7.33 ± 0.18) E-04	(6.5696 ± 0.0083) E-04
	236/233	(2.46 ± 0.16) E-04	(2.1510 ± 0.0060) E-04
	237/233	< 1.2 E-05	(7.2262 ± 0.57) E-06

U-233-2

	Ratio	96595	Pre-irradiated
		Ratio ± *U*	Ratio ± *U*
U233	233/233	---	---
	234/233	(7.878 ± 0.032) E-03	(1.7383 ± .0015) E-03
	235/233	(2.356 ± 0.014) E-03	(6.5696 ± 0.0083) E-04
	236/233	(2.38 ± 0.13) E-04	(2.1510 ± 0.0060) E-04
	237/233	< 1.2 E-05	(7.2262 ± 0.57) E-06

U-235-2

	m/z	96592	Pre-irradiated
		Ratio ± *U*	Ratio ± *U*
U235	234/235	(4.6849 ± 0.0084) E-04	
	235/235	---	---
	236/235	(1.1600 ± 0.0061) E-03	(5.9100 ± 0.012) E-04
	237/235	< 8.6 E-06	< 6.7E-07
	238/235	(4.282 ± 0.012) E-03	(8.4271 ± 0.028) E-04
	239/235	< 9.0 E-06	< 7.0E-07

U-235-1

	m/z	96591	Pre-irradiated
		Ratio ± *U*	Ratio ± *U*
U235	234/235	(6.566 ± 0.050) E-04	
	235/235	---	---
	236/235	(8.636 ± 0.045) E-03	(5.9100 ± 0.012) E-04
	237/235	< 8.3 E-04	< 6.7E-07
	238/235	(6.78 ± 0.60) E-03	(8.4271 ± 0.028) E-04
	239/235	< 7.0 E-04	< 7.0E-07

U-236-2

	m/z	96593	Pre-irradiated
		Ratio ± *U*	Ratio ± *U*
U236	236/236	---	---
	237/236	(1.0006 ± 0.0011) E-02	< 7.40e-06
	238/236	(1.5107 ± 0.0016) E-02	(1.4964 ± .0015) E-02
	239/236	(2.687 ± 0.033) E-04	(7.6 ± 3.1) E-06
	240/236	< 2.6 E-06	(8.3 ± 3.3) E-06

U-236-1

	m/z	96594	Pre-irradiated
		Ratio ± *U*	Ratio ± *U*
U236	236/236	---	---
	237/236	(1.296 ± 0.030) E-03	< 7.40e-06
	238/236	(1.9437 ± 0.0023) E-02	(1.4964 ± .0015) E-02
	239/236	(2.030 ± 0.016) E-03	(7.6 ± 3.1) E-06
	240/236	(9.61 ± 0.94) E-05	(8.3 ± 3.3) E-06

Np-237-1

	m/z	96621	Pre-irradiated
		Ratio ± *U*	Ratio ± *U*
Np237	236/237	(6.282 ± 0.052) E-06	
	237/237	---	---
	238/237	(1.7705 ± 0.0085) E-03	(5.455 ± 0.014) E-05
	239/237	< 4.6 E-06	(2.882 ± 0.200) E-05
	240/237	< 2.9 E -06	< 6.00 E-07
	241/237	< 3.3 E -06	< 6.10 E-07
	242/237	< 1.9 E-06	(3.069 ± 0.220) E-05

Np-237-5

	m/z	96619	Pre-irradiated
		Ratio ± *U*	Ratio ± *U*
Np237	236/237	(1.026 ± 0.010) E-05	
	237/237	---	---
	238/237	(4.185 ± 0.019) E-02	(5.455 ± 0.014) E-05
	239/237	(2.685 ± 0.049) E-04	(2.882 ± 0.200) E-05
	240/237	(1.41 ± 0.45) E-05	< 6.00 E-07
	241/237	< 4.8 E-06	< 6.10 E-07
	242/237	< 3.7 E-06	(3.069 ± 0.220) E-05

Np-237-4

	m/z	96620	Pre-irradiated
		Ratio ± *U*	Ratio ± *U*
Np237	236/237	(8.330 ± 0.073) E-06	
	237/237	---	---
	238/237	(3.223 ± 0.014) E-02	(5.455 ± 0.014) E-05
	239/237	(1.548 ± 0.076) E-04	(2.882 ± 0.200) E-05
	240/237	< 5.9 E-06	< 6.00 E-07
	241/237	< 6.1 E-06	< 6.10 E-07
	242/237	< 5.1 E-06	(3.069 ± 0.220) E-05

Np-237-2

	m/z	96622	Pre-irradiated
		Ratio ± *U*	Ratio ± *U*
Np237	236/237	(7.596 ± 0.068) E-06	
	237/237	---	---
	238/237	(2.0927 ± 0.0094) E-03	(5.455 ± 0.014) E-05
	239/237	< 5.6 E-06	(2.882 ± 0.200) E-05
	240/237	< 6.7 E-06	< 6.00 E-07
	241/237	< 4.5 E-06	< 6.10 E-07
	242/237	< 4.5 E-06	(3.069 ± 0.220) E-05

U-238-2

	m/z	96585	Pre-irradiated
		Ratio ± *U*	Ratio ± *U*
U238	237/238	(8.236 ± 0.074) E-06	(1.642 ± 0.058) E-06
	238/238	---	---
	239/238	(1.0267 ± 0.0046) E-02	< 9.50E-07
	240/238	(1.155 ± 0.097) E-04	<6.02E-07
	241/238	< 1.4 E-05	(1.051 ± 0.620) E-06
	242/238	< 7.3 E-06	(1.767 ± 0.100) E-05

U-238-1

	m/z	96586	Pre-irradiated
		Ratio ± *U*	Ratio ± *U*
U238	237/238	(9.092 ± 0.073) E-06	(1.642 ± 0.058) E-06
	238/238	---	---
	239/238	(7.266 ± 0.066) E-04	< 9.50E-07
	240/238	< 8.5 E-06	<6.02E-07
	241/238	< 9.7 E-06	(1.051 ± 0.620) E-06
	242/238	(1.53 ± .67) E -05	(1.767 ± 0.100) E-05

Pu-239-2

	m/z	96623	Pre-irradiated
		Ratio ± *U*	Ratio ± *U*
Pu239	239/239	---	---
	240/239	(1.290 ± 0.016) E-02	(2.2752 ± 0.0014) E-04
	241/239	(2.4764 ± 0.0059) E-03	< 5.70E-07
	242/239	(3.19 ± 0.15) E-04	(1.454 ± 0.066) E-05
	243/239	< 4.6E-06	< 4.30E-07

Pu-239-1

	m/z	96624	Pre-irradiated
		Ratio ± *U*	Ratio ± *U*
Pu239	239/239	---	---
	240/239	(1.150 ± 0.014) E-03	(2.2752 ± 0.0014) E-04

		241/239	< 5.0 E-06		< 5.70E-07
		242/239	(1.358 ± 0.088) E-04		(1.454 ± 0.066) E-05
		243/239	< 5.7 E-06		< 4.30E-07

Pu-240-3

	m/z	**96627**	**Pre-irradiated**
		Ratio ± *U*	**Ratio ± *U***
Pu240	240/240	---	---
	241/240	(2.93956 ± 0.00029) E-01	(3.2415 ± 0.0061) E-05
	242/240	(3.357 ± 0.067) E-03	(2.9433 ± 0.0180) E-04
	243/240	(7.04 ± 0.41) E-05	< 3.10E-07
	244/240	(1.020 ± 0.043) E-04	< 6.60E-07

Pu-240-1

	m/z	**96628**	**Pre-irradiated**
		Ratio ± *U*	**Ratio ± *U***
Pu240	240/240	---	---
	241/240	(7.331 ± 0.092) E-03	(3.2415 ± 0.0061) E-05
	242/240	(4.647 ± 0.086) E-04	(2.9433 ± 0.0180) E-04
	243/240	(1.51 ± 0.76) E-05	< 3.10E-07
	244/240	(2.21 ± 0.53) E-05	< 6.60E-07

Am-241-4

	m/z	**96616**	**Pre-irradiated**
		Ratio ± *U*	**Ratio ± *U***
Am241	238/241	(5.347 ± 0.056) E-02	(3.128 ± 0.056) E-04
	239/241	(4.02 ± 0.36) E-04	(3.45 ± 0.65) E-05
	240/241	(3.4 ± 3.1) E-05	< 3.8 E-06
	241/241	---	---
	242/241	(2.865 ± 0.030) E-02	(3.601 ± 0.047) E-05
	243/241	(5.8631 ± 0.0069) E-04	(1.82 ± 0.43) E-05
	244/241	(4.8 ± 2.8) E-05	< 4.1 E-06
	245/241	< 3.0 E-05	< 4.3 E-06

Am-241-3

	m/z	**96615**	**Pre-irradiated**
		Ratio ± *U*	**Ratio ± *U***
Am241	238/241	(6.860 ± 0.072) E-02	(3.128 ± 0.056) E-04
	239/241	(5.07 ± 0.30) E-03	(3.45 ± 0.65) E-05
	240/241	(5.70 ± 3.8) E-04	< 3.8 E-06
	241/241	---	---
	242/241	(4.209 ± 0.048) E-02	(3.601 ± 0.047) E-05
	243/241	(8.972 ± 0.061) E-04	(1.82 ± 0.43) E-05
	244/241	< 3.7 E-04	< 4.1 E-06
	245/241	< 2.8 E-04	< 4.3 E-06

Am-241-1

	m/z	**96617**	**Pre-irradiated**
		Ratio ± *U*	**Ratio ± *U***
Am241	238/241	(9.04 ± 0.120)E-03	(3.128 ± 0.056) E-04
	239/241	(3.22 ± 0.12) E-04	(3.45 ± 0.65) E-05
	240/241	< 2.1 E-05	< 3.8 E-06
	241/241	---	---
	242/241	(3.590 ± 0.057) E-03	(3.601 ± 0.047) E-05
	243/241	(8.1 ± 1.1) E-05	(1.82 ± 0.43) E-05
	244/241	< 2.7 E-05	< 4.1 E-06
	245/241	< 9.7 E-06	< 4.3 E-06

Am-241-2

	m/z	**96618**	**Pre-irradiated**
		Ratio ± *U*	**Ratio ± *U***
Am241	238/241	(1.511 ± 0.016) E-03	(3.128 ± 0.056) E-04
	239/241	(2.59 ± 0.28) E-04	(3.45 ± 0.65) E-05
	240/241	(1.04 ± 0.26) E-04	< 3.8 E-06
	241/241	---	---
	242/241	(9.79 ± 0.12) E-04	(3.601 ± 0.047) E-05
	243/241	< 2.2 E-05	(1.82 ± 0.43) E-05

	244/241	< 1.9 E-05	< 4.1 E-06
	245/241	< 2.5 E-05	< 4.3 E-06

Pu-242-3

	m/z	96600	Pre-irradiated
		Ratio ± *U*	Ratio ± *U*
Pu242	242/242	---	---
	243/242	(2.425 ± 0.017) E-02	(1.7824 ± 0.0051) E-05
	244/242	(1.2000 ± 0.0046) E-03	(2.2224 ± 0.0690) E-05
	245/242	(1.65 ± 0.64) E-05	< 7.60E-07
	246/242	< 4.1 E-06	< 8.6 E-07

Pu-242-4

	m/z	96599	Pre-irradiated
		Ratio ± *U*	Ratio ± *U*
Pu242	242/242	---	---
	243/242	(2.420 ± 0.017) E-02	(1.7824 ± 0.0051) E-05
	244/242	(1.1125 ± 0.0044) E-03	(2.2224 ± 0.0690) E-05
	245/242	(1.94 ± 0.60) E-05	< 7.60E-07
	246/242	< 4.7 E-06	< 8.6 E-07

Pu-242-1

	m/z	96601	Pre-irradiated
		Ratio ± *U*	Ratio ± *U*
Pu242	242/242	---	---
	243/242	(6.171 ± 0.043) E-04	(1.7824 ± 0.0051) E-05
	244/242	(1.59 ± 0.58) E-05	(2.2224 ± 0.0690) E-05
	245/242	< 6.4 E-06	< 7.60E-07
	246/242	< 4.5 E-06	< 8.6 E-07

Pu-242-2

	m/z	96602	Pre-irradiated
		Ratio ± *U*	Ratio ± *U*
Pu242	242/242	---	---
	243/242	(5.569 ± 0.039) E-04	(1.7824 ± 0.0051) E-05
	244/242	(9.2 ± 5.4) E-06	(2.2224 ± 0.0690) E-05
	245/242	< 5.1 E-06	< 7.60E-07
	246/242	< 4.7 E-06	< 8.6 E-07

Am-243-4

	m/z	96608	Pre-irradiated
		Ratio ± *U*	Ratio ± *U*
Am243	243/243	---	---
	244/243	(6.731 ± 0.071) E-02	(4.9261 ± 0.0180) E-05
	245/243	(1.126 ± 0.013) E-03	< 7.0 E-06
	246/243	< 1.7 E-05	< 6.1 E-06
	247/243	< 1.3 E-05	< 5.9 E-06

Am-243-1

	m/z	96609	Pre-irradiated
		Ratio ± *U*	Ratio ± *U*
Am243	243/243	---	---
	244/243	(1.821 ± 0.019) E-03	(4.9261 ± 0.0180) E-05
	245/243	< 4.3 E-05	< 7.0 E-06
	246/243	<3.9 E-05	< 6.1 E-06
	247/243	< 2.9 E-05	< 5.9 E-06

Am-243-3

	m/z	96607	Pre-irradiated
		Ratio ± *U*	Ratio ± *U*
Am243	243/243	---	---
	244/243	(6.539 ± 0.068) E-02	(4.9261 ± 0.0180) E-05
	245/243	(9.25 ± 0.14) E-04	< 7.0 E-06
	246/243	< 7.1 E-05	< 6.1 E-06
	247/243	(8.9 ± 5.7) E-05	< 5.9 E-06

Am-243-2

	m/z	96610	Pre-irradiated
		Ratio ± *U*	Ratio ± *U*

Am243	243/243	---	---
	244/243	(1.878 ± 0.020) E-03	(4.9261 ± 0.0180) E-05
	245/243	< 1.7 E-05	< 7.0 E-06
	246/243	< 1.7 E-05	< 6.1 E-06
	247/243	< 1.1 E-05	< 5.9 E-06

Pu-244-4

	m/z	96604	Pre-irradiated
		Ratio ± *U*	Ratio ± *U*
Pu244	244/244	---	---
	245/244	(2.021 ± 0.027) E-03	(2.0180 ± 0.0840) E-05
	246/244	< 4.1 E-06	< 4.80E-07
	247/244	< 4.2 E-06	<3.60E-07

Pu-244-5

	m/z	96603	Pre-irradiated
		Ratio ± *U*	Ratio ± *U*
Pu244	244/244	---	---
	245/244	(2.004 ± 0.026) E-03	(2.0180 ± 0.0840) E-05
	246/244	(1.10 ± 0.48) E-05	< 4.80E-07
	247/244	< 3.8 E-06	<3.60E-07

Pu-244-1

	m/z	96605	Pre-irradiated
		Ratio ± *U*	Ratio ± *U*
Pu244	244/244	---	---
	245/244	(4.029 ± 0.054) E-04	(2.0180 ± 0.0840) E-05
	246/244	< 4.1 E-06	< 4.80E-07
	247/244	< 4.5 E-06	<3.60E-07

Pu-244-2

	m/z	96606	Pre-irradiated
		Ratio ± *U*	Ratio ± *U*
Pu244	244/244	---	---
	245/244	(3.592 ± 0.048) E-04	(2.0180 ± 0.0840) E-05
	246/244	< 4.1 E-06	< 4.80E-07
	247/244	< 5.5 E-06	<3.60E-07

Cm-244-2

	m/z	96625	Pre-irradiated
		Ratio ± *U*	Ratio ± *U*
Cm244	240/244	(9.5922 ± 0.0046) E-02	(9.1259 ± 0.0036) E-02
	241/244	(1.9775 ± 0.0030) E-02	(3.86 ± 0.13) E-04
	242/244	(1.341 ± 0.043) E-03	(7.6 ± 1.1) E-05
	244/244	---	---
	245/244	(7.257 ± 0.096) E-02	(4.3541 ± 0.0190) E-02
	246/244	(2.43206 ± 0.00060) E-01	(2.3349 ± 0.0004) E-01
	247/244	(5.276 ± 0.025) E-03	(3.8519 ± 0.0089) E-03
	248/244	(2.480 ± 0.024) E-03	(2.2614 ± 0.0085) E-03

Cm-244-1

	m/z	96626	Pre-irradiated
		Ratio ± *U*	Ratio ± *U*
Cm244	240/244	(9.6720 ± 0.0046) E-02	(9.1259 ± 0.0036) E-02
	241/244	(1.9245 ± 0.0029) E-02	(3.86 ± 0.13) E-04
	242/244	(8.00 ± 0.26) E-04	(7.6 ± 1.1) E-05
	244/244	---	---
	245/244	(7.128 ± 0.095) E-02	(4.3541 ± 0.0190) E-02
	246/244	(2.43095 ± 0.00058) E-01	(2.3349 ± 0.0004) E-01
	247/244	(5.217 ± 0.031) E-03	(3.8519 ± 0.0089) E-03
	248/244	(2.401 ± 0.026) E-03	(2.2614 ± 0.0085) E-03

Cm-248-4

	m/z	96612	Pre-irradiated
		Ratio ± *U*	Ratio ± *U*
Cm248	248/248	---	---
	249/248	(8.986 ± 0.071) E-03	(3.1546 ± 0.018) E-05
	250/248	(3.783 ± 0.028)E-04	< 5.6 E-06

	251/248	(6.166 ± 0.062) E-05	< 4.8 E-06
	252/248	< 1.5 E-05	< 4.8 E-06

Cm-248-1

	m/z	96613	Pre-irradiated
		Ratio ± U	**Ratio ± U**
Cm248	**248/248**	---	---
	249/248	(4.865 ± 0.039) E-04	(3.1546 ± 0.018) E-05
	250/248	< 1.6 E-05	< 5.6 E-06
	251/248	< 1.5 E-05	< 4.8 E-06
	252/248	< 1.3 E-05	< 4.8 E-06

Cm-248-3

	m/z	96611	Pre-irradiated
		Ratio ± U	**Ratio ± U**
Cm248	**248/248**	---	---
	249/248	(8.347 ± 0.066) E-03	(3.1546 ± 0.018) E-05
	250/248	(3.26 ± 0.025) E-04	< 5.6 E-06
	251/248	(4.961 ± 0.051) E-05	< 4.8 E-06
	252/248	< 4.7 E-05	< 4.8 E-06

Cm-248-2

	m/z	96614	Pre-irradiated
		Ratio ± U	**Ratio ± U**
Cm248	**248/248**	---	---
	249/248	(4.709 ± 0.038) E-04	(3.1546 ± 0.018) E-05
	250/248	< 1.4 E-05	< 5.6 E-06
	251/248	< 2.3 E-05	< 4.8 E-06
	252/248	< 2.1 E-05	< 4.8 E-06

Eu-Cs_Rh-2

	Ratio	96587	Pre-irradiated
		Ratio ± U	**Ratio ± U**
Rh103	**103/103**	---	---
	104/103	(7.535 ± 0.052) E-04	(6.78 ± 0.55) E-06
	105/103	(6.06 ± 0.47) E-05	(6.61 ± 0.60) E-06
	106/103	(6.46 ± 0.57) E-05	(5.43 ± 0.73) E-06
Cs133	**133/133**	---	---
	134/133	(1.89847 ± 0.00071) E-02	< 8.3 E-06
	135/133	(1.118 ± 0.064) E-04	< 1.5 E-05
Eu153	**153/153**	---	---
	154/153	(6.332 ± 0.014) E-02	(4.176 ± 0.054) E-04
	155/153	(2.224 ± 0.024) E-03	< 9.80 E-04
	156/153	(4.22 ± 0.19) E-04	<8.40 E-04

Eu-Cs_Rh-1

	Ratio	96588	Pre-irradiated
		Ratio ± U	**Ratio ± U**
Rh103	**103/103**	**---**	---
	104/103	(4.41 ± 0.41) E-04	(6.78 ± 0.55) E-06
	105/103	(5.41 ± 0.71) E-04	(6.61 ± 0.60) E-06
	106/103	(2.66 ± 0.38) E-04	(5.43 ± 0.73) E-06
Cs133	**133/133**	---	---
	134/133	(6.49 ± 0.41) E-04	< 8.3 E-06
	135/133	< 4.6 E-05	< 1.5 E-05
Eu153	**153/153**	---	---
	154/153	(2.7191 ± 0.0058) E-03	(4.176 ± 0.054) E-04
	155/153	(6.7 ± 2.3) E-05	< 9.80 E-04
	156/153	(1.1015 ± 0.2110) E-04	<8.40 E-04

Sm-Ru-Nd-5

	Ratio	96597	Pre-irradiated
		Ratio ± U	**Ratio ± U**
Ru101	**101/101**	---	---
	102/101	(2.1894 ± 0.0071) E-02	(1.4562 ± 0.0001) E-02
	103/101	(1.586 ± 0.022) E-03	(5.43 ± 0.24) E-05
Nd143	**143/143**	---	---

	Ratio		
	144/143	(5.7102 ± 0.0014) E-02	(4.9421 ± 0.0001) E-02
	145/143	(7.3595 ± .0097) E-03	(7.2540 ± 0.0007) E-03
	146/143	(1.6424 ± 0.0010) E-02	(1.6169 ± 0.0001) E-02
Sm149	**149/149**	---	---
	150/149	(5.79472 ± 0.00080) E-01	(5.7171 ± 0.0170) E-03
	151/149	(4.234 ± 0.025) E-03	< 1.3 E-05
	152/149	(5.852 ± 0.030) E-03	(3.9957 ± 0.0180) E-03

Nd-Pd-4

		96598	Pre-irradiated
	Ratio	**Ratio ± *U***	**Ratio ± *U***
Pd105	**105/105**	---	---
	106/105	(4.3138 ± 0.0013) E-02	(3.8391 ± 0.0002) E-02
	107/105	(2.679 ± 0.071) E-04	(1.9945 ± 0.0066) E-04
	108/105	(3.636 ± 0.011) E-03	(3.2999 ± 0.0006) E-03
Nd145	**145/145**	---	---
	146/145	(5.74473 ± 0.00053) E-02	(4.7990 ± 0.0001) E-02
	147/145	(1.0497 ± 0.0038) E-03	(9.8693 ± 0.0084) E-04

Sm-6

		96629	Pre-irradiated
	Ratio	**Ratio ± *U***	**Ratio ± *U***
Sm149	**149/149**	---	---
	150/149	(1.0215 ± 0.0031) E-02	(5.7171 ± 0.0170) E-03
	151/149	(5.1 ± 2.3) E-05	< 1.3 E-05
	152/149	(3.997 ± 0.025) E-03	(3.9957 ± 0.0180) E-03

5.3. Results – U-235 wires

The U-235 flux wires were also analyzed at INL's Analytical Lab. Gamma spectrometry as well as Quadrupole ICP-MS were used to determine the absolute amount of Cs-137 and Nd-148 in the wires (MC-ICP-MS provides only isotopic ratios not absolute values).

The 2-sigma uncertainties associated to the gamma and Q-ICP-MS measurements are, respectively, 1% and 5%. These measurements show that the neutron flux in the Cd-filtered irradiation is close to being symmetric which is what is expected based on our knowledge of the reactor. On the other hand, the wires present in the 5-mm- and 10-mm-boron-filtered irradiation show a significant asymmetry of the neutron flux which is **currently not fully understood** and is still subject to investigations.

Table 5.2: Characterization of the irradiated U-235 wires with gamma spectrometry and Q-ICP-MS

	AL sample nº	Cs-137 (Gamma)	Mass 137 (Q-ICP-MS)	Mass 148 (Q-ICP-MS)
		µCi/wire	µg/wire	µg/wire
Cd filter	**96577**	61.30	0.6980	0.2180
	96578	78.80	0.9000	0.2850
	96579	74.80	0.8550	0.2700
	96580	65.80	0.7450	0.2330
5-mm-B filter	**96581**	7.00	0.0753	0.0216
	96582	16.20	0.2020	0.0600
	96583	11.50	0.1520	0.0420
	96584	6.84	0.0875	0.0241
10-mm-B filter	**97939**	4.99	0.0604	0.0170
	97940	7.90	0.0950	0.0269
	97941	5.56	0.0688	0.0189
	97942	6.11	0.0745	0.0209

From these measurements, knowing the mass of U-235 in each wire, it is possible to infer the atom ratios necessary to normalize the flux calculations. Table 5.3 shows that the Cs-137 over U-235 atom ratios obtained from gamma and Q-ICP-MS measurements are very similar, which is a reassuring sanity check.

Table 5.3: Inferred Cs-137 and Nd-148 over U-235 atom ratios in the U-235 wires

	AL sample n°	Cs-137/U-235 (Gamma)	Mass 137/U-235 (Q-ICP-MS)	Mass 148/U-235 (Q-ICP-MS)
		Atom ratios		
Cd filter	96577	9.38E-04	9.24E-04	2.67E-04
	96578	1.15E-03	1.13E-03	3.32E-04
	96579	1.16E-03	1.15E-03	3.36E-04
	96580	9.93E-04	9.73E-04	2.82E-04
5-mm-B filter	96581	9.02E-05	1.02E-04	2.71E-05
	96582	2.42E-04	2.61E-04	7.17E-05
	96583	1.69E-04	1.94E-04	4.95E-05
	96584	9.69E-05	1.07E-04	2.73E-05
10-mm-B filter	97939	7.47E-05	7.83E-05	2.04E-05
	97940	1.18E-04	1.23E-04	3.23E-05
	97941	8.33E-05	8.91E-05	2.27E-05
	97942	9.15E-05	9.65E-05	2.51E-05

6. ATR AS-RUN PHYSICS CALCULATIONS WITH MCNP

The objectives of the physics calculations are the following:

- Perform detailed Monte Carlo neutron transport calculations of the tests in the ATR
- Minimize approximations
- Develop a multi-step transport process/techniques/models
- Calculate very accurate one-group neutron cross sections (<0.5%)
- Understand the sensitivities affecting the 1-group cross sections
- Deplete rodlet samples using:
    - Measured ATR reactor data
    - Calculated 1-group neutron cross sections
    - Measured initial sample isotopic masses
    - Calculated irradiation flux (re-normalized per measured fluence wires)
- Compare measured versus calculated isotopics (A+1)/A ratios in the irradiated samples

6.1. The MCNP code

MCNP is a general purpose, continuous energy, generalized geometry, and coupled neutron-photon-electron Monte Carlo transport code. Neutrons and gamma-rays are typically and routinely transported using the MCNP code for applications related to ATR analyses. A wide variety of nuclide cross sections and nuclear reactions are available from the ENDF. The MCNP code is a product of the Los Alamos National Laboratory.

The MCNP code can handle a variety of nuclear interactions for neutrons with nuclei usually only limited by the data available on ENDF and the MCNP ACE cross section files (ACE is an acronym for A Compact ENDF or processed cross section data specifically for use by MCNP). Typically, all MCNP ACE files include the following neutron reaction cross sections: total, elastic scattering, inelastic scattering, fission, radiative capture, (n,2n), (n,p), (n,a), and (n,p). Other cross sections may be provided as well depending on important nuclear interaction characteristics of a particular nucleus. In addition, for neutron inelastic and radiative capture reactions, MCNP will produce de-excitation gamma-rays and track these gamma-rays in the photon portion of the transport calculation.

The models used in MCNP represent a system's physical geometry with a collection of volumetric cells described by defined geometric surfaces (planes, cylinders, spheres, cones, etc.). These code-recognizable defined surfaces are appropriately combined and sensed to allow the analyst wide latitude in describing even very complicated three-dimensional system geometries. A complex reactor system, such as the ATR, is readily transformed into an MCNP cell geometry model (although thousands of cells are typically needed to fully describe the entire ATR core). The MCNP code also requires the model cells to contain a material. This material is composed of natural or isotopic elements that describe the cell material. An elemental or isotopic number density and associated neutron and/or photon cross section library are required for each element or isotope.

The MCNP cell tally capability allows for the calculation of a variety of reactor physics parameters. For example, one can calculate particle or energy currents and fluxes in any cell, or across any cell surface. Nuclear reaction rates (e.g., fission or radiative capture reaction rates) can be calculated in any cell. Similarly, energy deposition due to neutron scattering or absorption and gamma-ray scattering events (heating rates) can also be calculated. In addition, these tally quantities can be calculated as a function of energy group to determine spectral characteristics of certain reaction and heating rates. Cell tallies are averaged over the cell's volume and possess an inherent Monte Carlo statistical error.

Because the MCNP computer code is a Monte Carlo code, the MCNP-calculated results are reported by the code with an associated statistical uncertainty or relative error. The relative errors translate into a one-sigma statistical uncertainty by multiplication of the relative error by the calculated result (tally value). Two-sigma and three-sigma confidence intervals are obtained by multiplying the one-sigma values by factors of two and three, respectively. The confidence levels associated with one-, two-, and three-sigma values are 68.3%, 95.4%, and 99.7%, respectively.

6.2. ATR MCNP model

The main goal of the MANTRA physics modeling was to calculate appropriate one-group neutron cross sections, reaction rates, and fluxes at each MANTRA sample location. So far, the MANTRA-1 (thin boron filter) and the MANTRA-3 (cadmium filter) experiments have been modeled and analyzed. The MANTRA-1 experiment had 25 sample locations and MANTRA-3 had 28 sample locations. The one-group neutron cross sections and fluxes are then used as input for the sample depletions in order to estimate the end-of-irradiation sample concentrations and compare them with the measured concentrations.

The Monte Carlo physics depletion analysis is a multi-step process that begins with the construction of a detailed, fully-explicit, three-dimensional full-core model of the Advanced Test Reactor (ATR) and the particular MANTRA experiment. Figure 6.1 shows three MCNP plots: (1) cross sectional view of the ATR core model, (2) magnified cross section view of the B9 test facility in the north beryllium reflector region, and (3) an even greater magnified cross sectional view of the MANTRA-1 test train. All three plots are from the MCNP ATR model for the MANTRA-1 experiment. The MCNP model contains the serpentine ATR driver fuel, nine flux traps, surrounding experiments, beryllium reflector, outer shim control cylinders (orange circles), neck shim housing, neck shim rods, ATR pressure vessel, and the MANTRA-1 experiment. The ATR driver fuel is loaded based on the actual element loadings specified prior to each ATR irradiation power cycle.

The second step is the Monte Carlo depletion of the ATR driver core. The ATR driver fuel in the MCNP model is then depleted on a daily-basis over the appropriate number of ATR cycles and daily timesteps in which the MANTRA experiment was irradiated. The JMOCUP depletion utility program is used to perform the depletion calculation which incorporates the MCNP code and the ORIGEN2.2 computer code. The JMOCUP depletion calculations deplete the driver core (40 fuel elements or 840 cells) on a daily timestep basis taking into account the daily-average rotation of the ATR outer shim control elements and the daily neck shim removals. The MCNP KCODE calculation produces a k-effective close to 1.0 over the cycle. In addition to the driver core depletion, the MANTRA filters are also depleted (boron or cadmium). The MANTRA-1 experiment was irradiated for two ATR cycles (151B and 152B), whereas the MANTRA-3 experiment was irradiated for only one cycle (152B). There were 57 timesteps for cycle 151B and 53 timesteps for 152B which creates 57 and 52 MCNP input/output files; each MCNP input model is approximately 100,000 lines long.

Because the MANTRA filters tend to absorb the bulk of the neutrons, very few of the fission neutrons produced in the ATR driver core or fission neutrons that thermalize in the beryllium reflector actually penetrate to the MANTRA samples. This results in only a small percentage of starting neutrons producing nuclear interactions with the samples leading to difficulties producing converged tally results. Plus, sample tally volumes are very small; the vial volume is approximately 0.017 cm^3 and the actual samples take up less than 0.005 cm^3 which further exacerbates the tally convergence. With relatively few neutrons making it to the samples and the small sample volumes, the neutron transport must now rely on a fixed source problem to accurately estimate the sample fluxes and reaction rates. Fixed source problems have the advantage of pushing large numbers of particles through the model core geometry and scaling runtime to the number of computer CPUs. Large number of CPUs and starting particles can then produce the tight tally convergence (<0.25%) required for MANTRA.
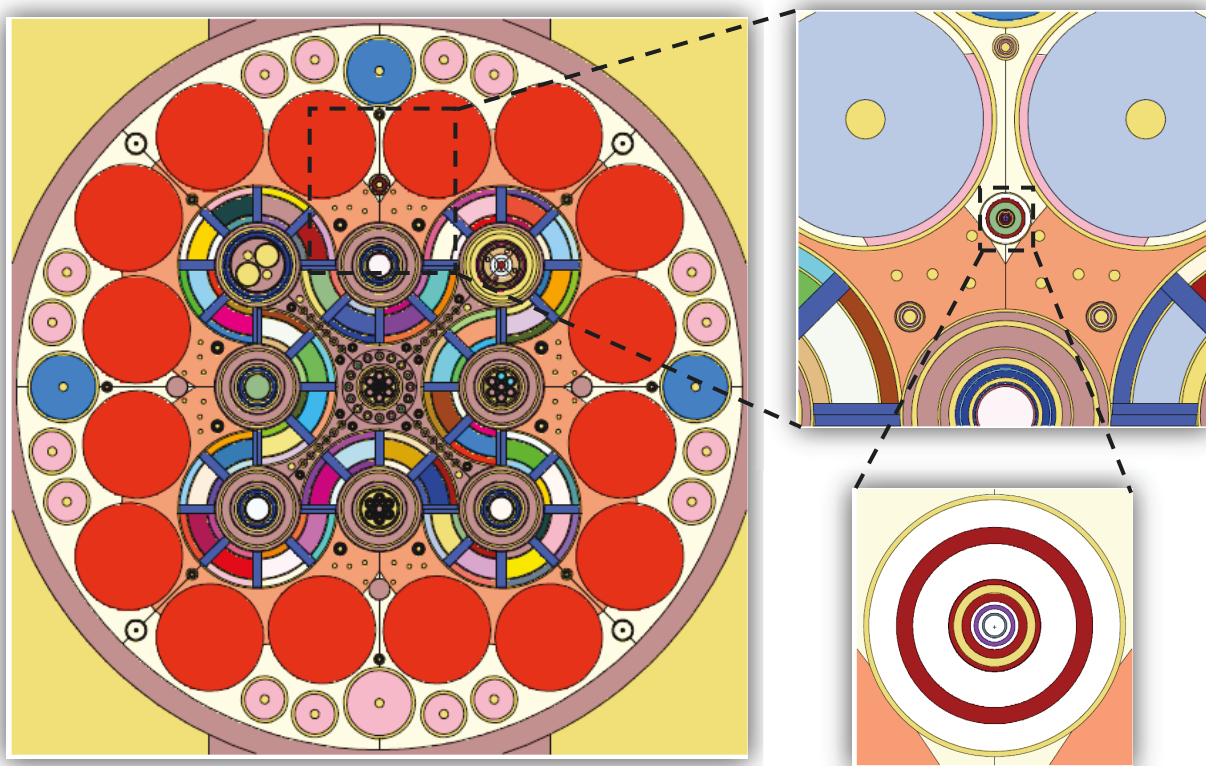
Figure 6.1. Details of the ATR MCNP model

The third step in the physics analysis is the development of the fixed source MCNP model of the ATR core. The KCODE MCNP models were converted to fixed source using the ATR driver fuel fission densities from the KCODE analysis and converting these fission densities into fission source probabilities or fission neutron starting points. The fixed source models could run many more starting particles than the KCODE models and hence could achieve much better tally statistics in the rodlet sample stacks. The fixed source models typically ran 200 billion particles on 2080 CPUs on the INL supercomputers which still took approximately 2 days per run. The tally statistics for the sample fluxes, reaction rates, and one-group unperturbed, infinite dilute cross sections were <0.25%.

The fourth step was the depletion of the sample compositions using the ORIGEN2.2 computer code. The fixed source model fluxes and one-group cross sections were part of the ORIGEN2.2 input data along with the measured initial sample isotopic compositions (Table 5.1). The samples were depleted for the respective irradiation periods with the daily irradiation fluxes normalized to the daily ATR lobe power. The end-of-irradiation sample compositions were then compared to the measured values given in Table 5.1. Calculated-to-experimental (C/E) ratios were then estimated.

The first set of ATR MCNP as-run analyses did not take into account the actual actinide mass of the samples because it was thought to be an inconsequential parameter for the determination of the isotopic ratios in the irradiated samples. In other words, the mass of actinides in the samples was consid-

ered infinitesimal, i.e. for all practical purpose zero. This modeling assumption is standard and valid in many instances. It also greatly simplifies the modeling of the experiments.

However, in the case of the MANTRA experiment, the comparison of the measured ratios (see Table 5.1) with the results of these first MCNP calculations showed large discrepancies. The investigations carried out to understand the origin of these discrepancies quickly converged on the assumption of an infinitesimal sample mass. Indeed, considering an infinitesimal sample mass for the MANTRA experiment is a significant source of errors for certain isotopes because of a fundamental neutron physics phenomenon: the energy self-shielding. This aspect is presented in more detail in the following section.

6.3 Modeling the neutron energy self-shielding in the samples

The neutron energy self-shielding phenomenon finds its origin in the resonance structure of most actinide cross-sections. In the resonance energy region, from roughly 1 eV to 100 keV, the main absorption of neutrons by heavy nuclei takes place at relatively sharply defined resonance energies. A typical example of the cross-section variation in the resonance region is provided by uranium-238 (Figure 6.2).

If the amount of material is large enough the pronounced resonance structure of neutron cross sections leads to a corresponding fine structure in the neutron flux. If there is enough material there will be dips in the neutron flux at those energies (and locations) where there is strong resonance absorption or scattering (Figure 6.3).
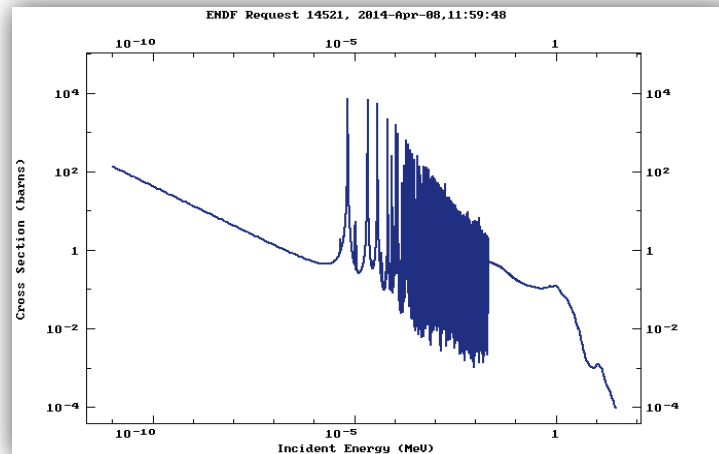

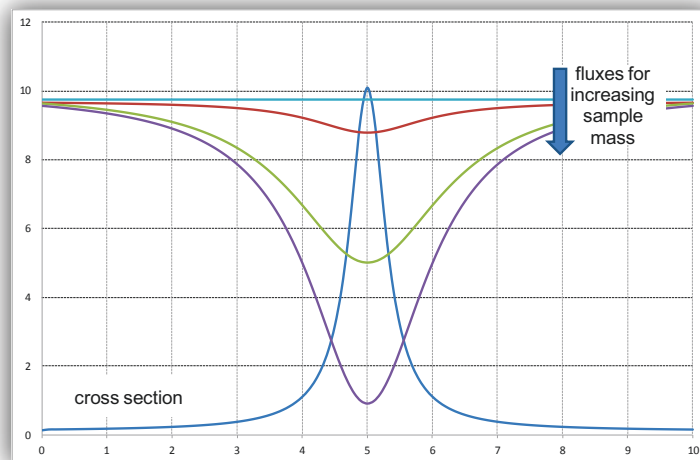Figure 6.2. Neutron capture cross-section of uranium-238 as a function of neutron energy

Figure 6.3. Illustration of neutron flux dip caused by a neutron resonance as the sample mass increases

The neutron energy self-shielding causes the neutron reaction rates in a material to be a non-linear function of the mass of material. Indeed, if the amount of material is sufficient, it will experience neutron energy self-shielding and, consequently, the neutron reaction rate R will be expressed as

$$R = \int [N \times \sigma(E) \times \varphi(E, N, g)]dE$$

where the neutron flux $\varphi(E, N, g)$ depends on the neutron energy E, on the amount of material present N, and to a lesser extent on the geometrical configuration g. As illustrated in Figure 6.3, when the sample mass reaches in certain value, the neutron flux will exhibit a larger and larger dip as the sample mass increases. In these situations adding more mass to a sample increases the reaction rates less than proportionately, i.e.

$$R(\alpha N) < \alpha R(N)$$

On the other hand, if the amount of material is small enough it will not experience neutron energy self-shielding. The neutron flux is not impacted by the presence of the sample material. In this case the neutron reaction rate will be expressed as

$$R = \int [N \times \sigma(E) \times \varphi(E)]dE$$

where the neutron flux $\varphi(E)$ depends only the neutron energy E and not on the (very small) amount of material. In these situations adding more mass to a sample increases the reaction rates proportionately, i.e.

$$R(\alpha N) = \alpha R(N)$$

Whenever possible, the latter situation is preferred because less detail is required for modeling the samples accurately. In particular, **it makes isotopic ratios in irradiated samples independent of the initial mass of material**.

To obtain a more detailed understanding of the neutron physics of the experiment, the reaction rates in the samples have been decomposed as a function of the neutron energy for each sample (see examples in Figure 6.4 to 6.6). This approach allows pin-pointing which energy region is responsible for the neutron interactions in a given sample and will guide the self-shielding analysis by providing the important energy ranges for each sample/filter combination.
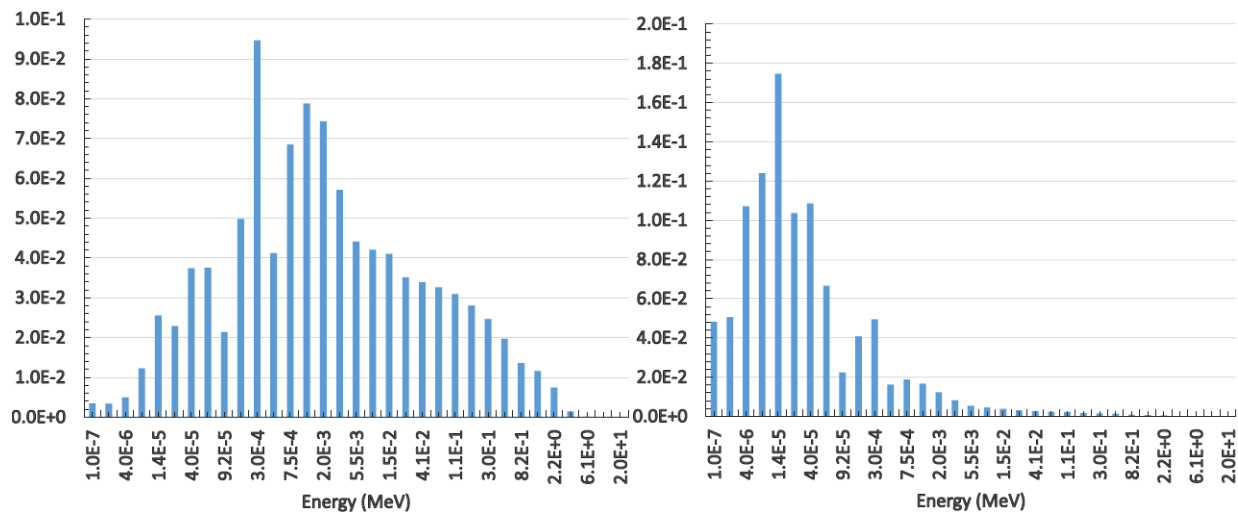

Figure 6.4. Normalized capture reaction rate in a U-235 sample filtered with 5-mm enriched boron (left) and cadmium (right)
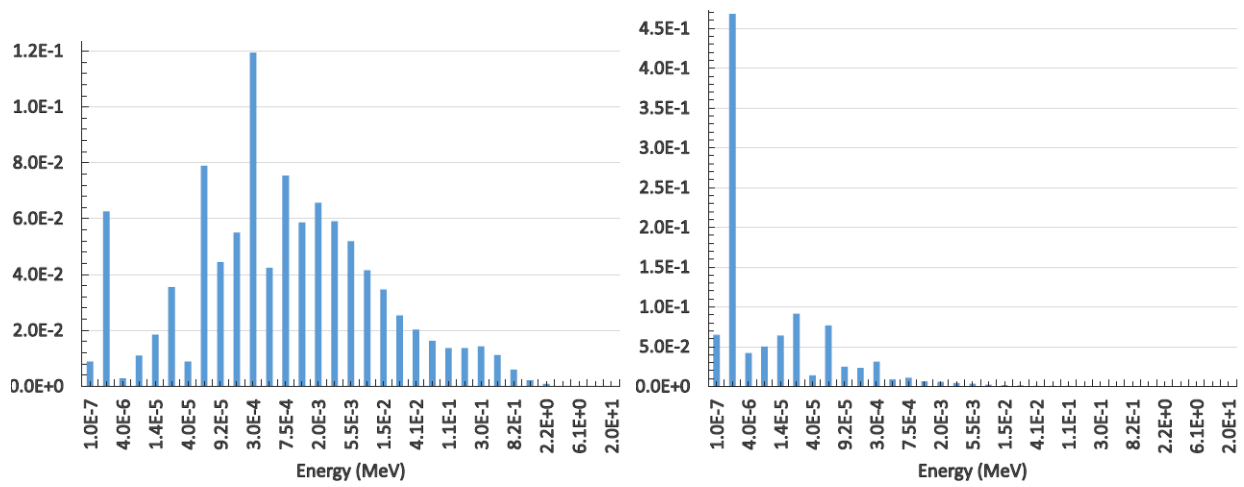
Figure 6.5. Normalized capture reaction rate in an Pu-239 sample filtered with 5-mm enriched boron (left) and cadmium (right)
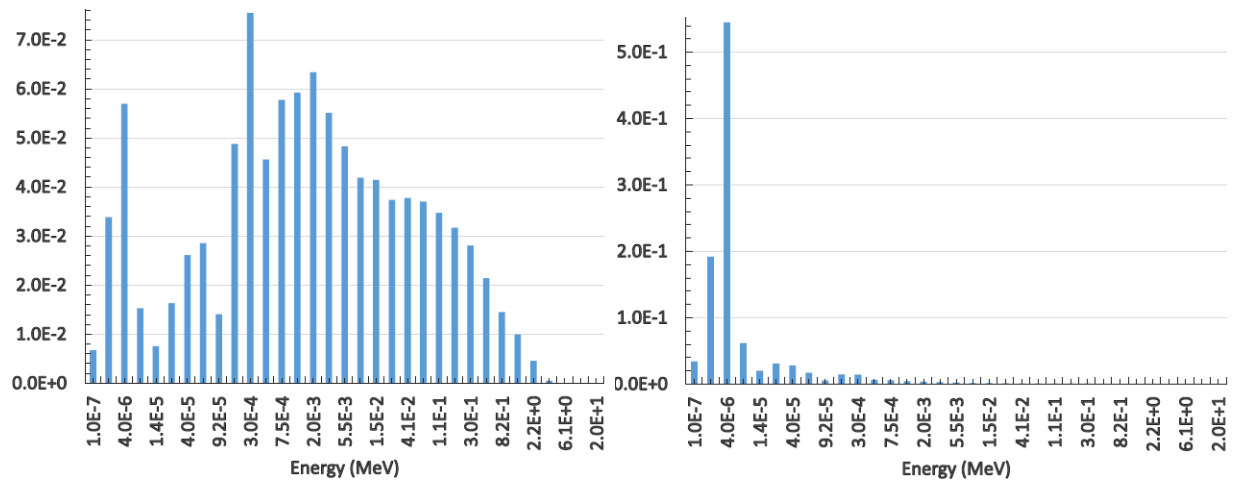

Figure 6.6. Normalized capture reaction rate in an Am-241 sample filtered with 5-mm enriched boron (left) and cadmium (right)

7. COMPARISON BETWEEN CALCULATIONS AND EXPERIMENT

This section presents the results of the analyses carried out for the cadmium-filtered samples. The analyses for the two boron-filtered irradiations are still underway, in particular to understand the axial asymmetry of the flux. The calculations related to the cadmium-filtered irradiations showed that the neutron spectra are practically independent of the axial position (see figure 7.1) and burn up conditions (see figure 7.2). The MCNP calculations provided one group cross sections, with low statistical uncertainty (typically less than 0.5%) to be subsequently used in a burn up code for calculating the isotope build up due to neutron irradiation.

The hypothesis made in the Monte Carlo calculations was that infinite dilution cross sections could be used. However, as mentioned earlier, it was soon realized that although the masses (typically in the 1mg range) were small, still significant self-shielding effects were present, especially for those isotopes with large resonances in the epithermal spectrum that was produced at the sample location by the Cd filter.
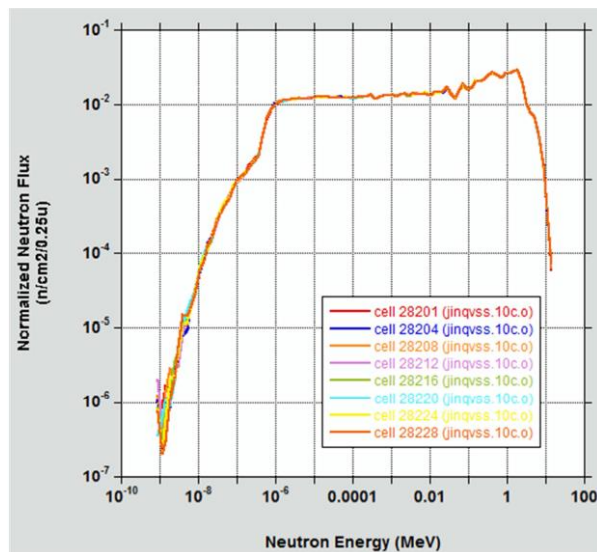

Figure 7.1. MANTRA Cd filtered neutron spectra axial independence (different cell numbers correspond to different axial locations).
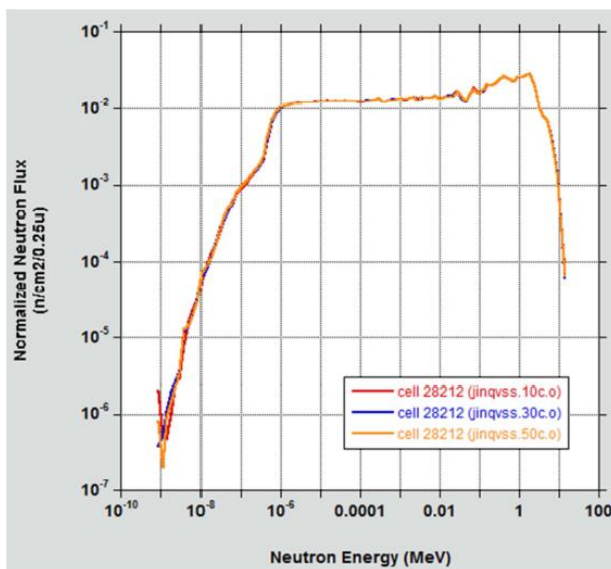

Figure 7.2. MANTRA Cd filtered neutron spectra burn up independence (different identifier numbers correspond to different number of days of irradiation).

33

The self-shielding effects are both energy and geometry dependent. To quantify the effect of the geometry, different wafer heights were explicitly modeled (Figure 7.3), each wafer containing the same amount of material. This allowed quantifying the dilution effects. Figure 7.4 shows, for instance, the effective capture cross section dependence of the Pu-240 sample in function of the mass and the height (occupied volume in the capsule). Unfortunately, at the moment of the sample preparation a large uncertainty (typically ~30%) was associated to the mass sample. This mass sample was measured after the PIE with a lot more precision (~1%) but the original volume was not known because the sample was dissolved. In practice, the unknown quantity was the original sample density. In order to cope with this problem a strategy was devised for calculating the most reliable C/E for the sample cross sections. This is detailed in the following.
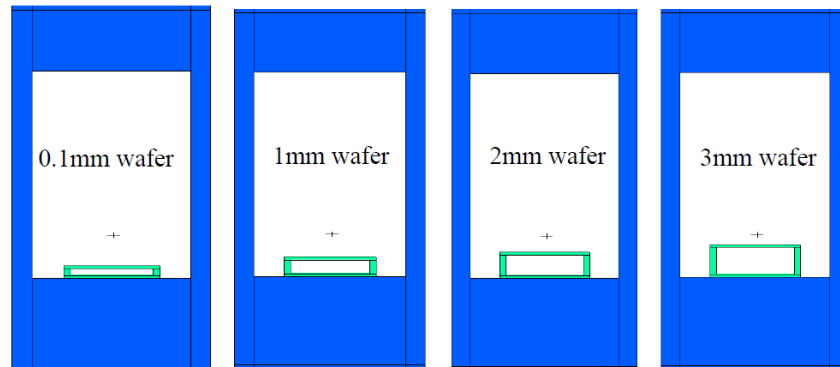

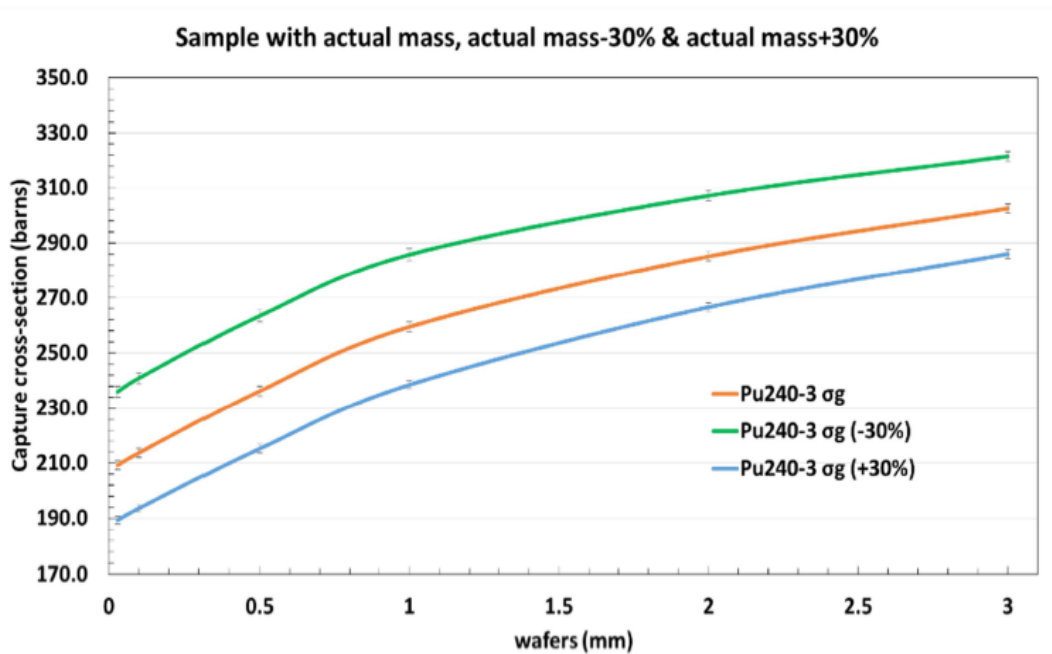Figure 7.3. Sample wafer with different heights inside a rodlet

Figure 7.4. Cadmium-filtered effective Pu-240 capture cross section dependence form sample mass and height in the capsule (wafer).

Starting points are the fluxes calculated using the detailed MCNP model (~ hundreds billions of histories), ENDF/B-VII.0 cross sections, and total ATR power from thermal-hydraulics measurements. In the next step flux normalization factor is calculating using 6 burn up indicators measured in 4 different wires: 137Cs (gamma) and buildup of 137Cs+137Ba, 139La, 145Nd, 146Nd, and 148Nd. Final factor is calculated by inverse weighting of square of the uncertainty. Following this step the MCNP fluxes are normalized with the obtained factor. It was checked that nonlinear effect (i.e. recalculation of normalization factor using the normalized fluxes) is negligible (~0.2%). These normalized fluxes are used in the

Bateman equation solver for calculating the sample isotope buildup due to irradiation. Dispersion of results is ~±2% (results regarding the burn up indicators are shown in table 7.1 for the second iteration, used for checking nonlinear effect).

Table 7.1. Wires C/E for determining flux normalization factor (second iteration). Normalization Factor=1.002 ± 2.06%.

Wire Location	^{137}Cs (γ)	Experim. Unc.	^{137}Cs $(+^{137}Ba)$	Experim. Unc.	^{139}La	Experim. Unc.	^{145}Nd	Experim. Unc.	^{146}Nd	Experim. Unc.	^{148}Nd	Experim. Unc.
4	1.00	1.04%	1.05	2.50%	1.00	0.75%	0.97	0.75%	0.99	0.75%	0.99	2.50%
11	1.01	0.98%	1.06	2.50%	1.00	0.75%	0.97	0.75%	0.99	0.75%	0.98	2.50%
19	1.02	1.16%	1.07	2.50%	1.01	0.75%	0.98	0.75%	1.00	0.75%	0.99	2.50%
26	1.03	1.00%	1.09	2.50%	1.03	0.75%	1.00	0.75%	1.02	0.75%	1.02	2.50%

The next step deals with the crucial task of determining the effective (self-shielded cross sections). Indication from the experiment preparation was that actual height of the sample should vary between 0.1 mm and 3mm. Moreover, the actual masses with low uncertainty were provided by the PIE results. Therefore, a parametric cross section calculations was performed corresponding to: 0.1 mm, 0.5mm, 1mm, 2mm, and 3mm. Using these cross sections, C/E for capture cross section were determined by iterative process changing the capture cross section in the Bateman equation until the measured build up is matched. This method is more accurate than traditional one (i. e. just using ratio of A+1/A densities) especially when the father is the A+1 isotope, A+2, or higher.

Sample height was determined by consistency (within uncertainty) of C/E for samples when the father is isotope A, and then when the father is isotope A+1. In fact in the case of the A+1 father, because the produced build up is a very negligible mass, practically no self-shielding effect is present. This very lengthy process (several hundreds of burn up calculations) allowed determining the height of the sample which was found to be dependent on the initial chemical form of the sample. Actually, there were two main chemical forms: oxide and nitrate. The height of the oxide was found to be close to 0.1 mm, whereas for the nitrate form was 0.35mm.

Table 7.2 and 7.3 summarize the obtained C/E respectively for the actinides samples and fission product samples. It has to be pointed out that there are four components, statistically combined, used in calculating the uncertainty associated to the C/E. The four components are:

- Experimental from PIE measurements (typically less than 0.5%)
- Statistical form the Monte Carlo calculations (typically less than 0.5%)
- Flux normalization factor dispersion (~2%)
- Effective (self-shielded) cross sections depending on the amount of self-shielding (varying from 1 to 3% uncertainty).

As mentioned in section 2.1, the sensitivity of the A+1 atom density with regards to the capture cross section of isotope A is very close to 1. In other words, a 1% difference between the calculated and measured A+1 density after irradiation implies a 1% difference between the calculated effective capture cross section of A and the "true" one.

The C/E yellow flagged are still under investigation regarding inconsistencies either in the measured mass of the father, or the measured mass of the daughter. Subsequent measurements regarding these dubious results are expected soon.

Table 7.2. Actinide C/E for capture cross sections

Isotope	Sample Position	Type	σ_g C/E	Experimental Uncertainty	C/E Uncertainty
^{232}Th	13	A	0.74	0.24%	3.50%
^{233}U	6	A	1.12	0.21%	2.38%
^{235}U	7	A	0.97	0.28%	2.40%
^{236}U	24	A	1.24	0.05%	4.40%
^{237}Np	3	A	0.93	0.22%	2.41%
	16	A	0.97	0.23%	2.42%
^{238}U	20	A	1.09	0.22%	4.21%
^{238}Pu	3	A+1	1.11	3.12%	4.11%
	16	A+1	1.01	1.02%	2.87%
^{239}Pu	20	A+1	0.81	4.20%	4.90%
	23	A	1.07	0.62%	3.77%
^{240}Pu	23	A+1	1.00	0.63%	3.13%
	14	A	1.06	0.01%	3.96%
Isotope	Sample Position	Type	σ_g C/E	Experimental Uncertainty	C/E Uncertainty
^{241}Am	15	A	0.84	0.52%	2.51%
	27	A	0.83	0.52%	2.47%
^{242}Pu	9	A	1.01	0.70%	4.87%
	25	A	0.95	0.70%	4.87%
^{243}Am	9	A+1	0.89	0.19%	2.73%
	25	A+1	0.91	0.19%	2.73%
	5	A	1.00	0.52%	3.12%
	21	A	0.84	0.52%	3.76%
^{244}Pu	10	A	2.74	0.67%	3.40%
	17	A	2.91	0.65%	3.41%
^{244}Cm	5	A+1	1.09	0.92%	4.22%
	21	A+1	1.03	0.78%	4.36%
	12	A	1.11	5.09%	6.86%
	22	A	1.12	5.09%	6.85%
^{248}Cm	8	A	0.98	0.39%	4.23%
	18	A	0.92	0.40%	4.20%

Table 7.3. Fission products C/E for capture cross sections

Isotope	Sample Position	Type	σ_g C/E	Experimental Uncertainty	C/E Uncertainty
[105]Pd	1	A	0.85	0.14%	2.59%
[145]Nd	1	A	1.01	0.03%	2.85%
[143]Nd	2	A	0.92	0.09%	2.49%
[101]Ru	2	A	0.63	0.48%	2.90%
[149]Sm	2	A	0.95	0.01%	3.22%
[103]Rh	28	A	?	0.35%	2.59%
[133]Cs	28	A	0.96	0.19%	2.99%
[153]Eu	28	A	1.02	0.11%	2.41%

8. CONCLUSIONS

This report presents the status of the MANTRA integral reactor physics experiment whose objective is to infer the effective neutron capture cross-sections for most of the actinides of importance for reactor physics and fuel cycle studies in both fast and epithermal spectra. Some fission products are also being considered. This experimental program has been funded by the ATR National Scientific User Facility (ATR-NSUF) and by the DOE Office of Science in the framework of the Recovery Act.

The principle of the experiment is to irradiate very pure actinide samples in the Advanced Test Reactor at INL and, after a given time, determine the amount of the different transmutation products. The determination of the nuclide densities before and after neutron irradiation will allow inference of effective neutron capture cross-sections. The list of actinides that were irradiated is the following: Th-232, U-233, U-235, U-236, U-238, Np-237, Pu-239, Pu-240, Pu-242, Pu-244, Am-241, Am-243, Cm-244 and Cm-248. The list of fission products is the following: Sm-149, Eu-153, Cs-133, Rh-103, Ru-101, Nd-143, Nd-145and Pd-105.

In order to obtain effective neutron capture cross sections corresponding to different neutron spectra, three sets of actinide samples have been irradiated: the first one is filtered with **cadmium** and the other two are filtered with **enriched boron** of different thicknesses (5 mm and 10 mm). This allowed the samples to be irradiated in epithermal and fast neutron spectra whereas the unfiltered neutron spectrum is largely thermal. The cadmium-filtered and the 5-mm-boron-filtered irradiations were completed in January 2013 after, respectively, 55 days and 110 days in the reactor. The last irradiation with the 10-mm boron filter was completed in January 2014 after approximately 110 days in the reactor.

The measurements of the isotopic ratios in the irradiated samples were carried out at the Materials and Fuels Complex (MFC) using the newly acquired Multi-Collector Inductively Coupled Plasma Mass Spectrometer (MC-ICP-MS). As of today, the MC-ICP-MS analyses have been completed for the samples irradiated with the 5-mm-boron filter and with the cadmium filter. The MC-ICP-MS analyses for the samples irradiated with the 10-mm-boron filter will be completed during in FY15.

The first analyses of the MANTRA experimental results of the cadmium filter configuration are encouraging. In particular, a premiere has been achieved for the evaluation of Pu-244 and Cm-248 never measured before with an integral experiment. Some lessons have been learned and will be taken into account for future experimental campaigns. In particular: (1) Improve sample preparation to know the ex-

perimental conditions better: density and geometry, (2) Further minimize the sample masses and (3) Improve wire characterization and choice of detectors.

Once the best-estimate MCNP calculations are finalized MANTRA will contribute to an iterative process involving reactor physicists and nuclear data evaluators necessary to the generation of accurate nuclear data files.
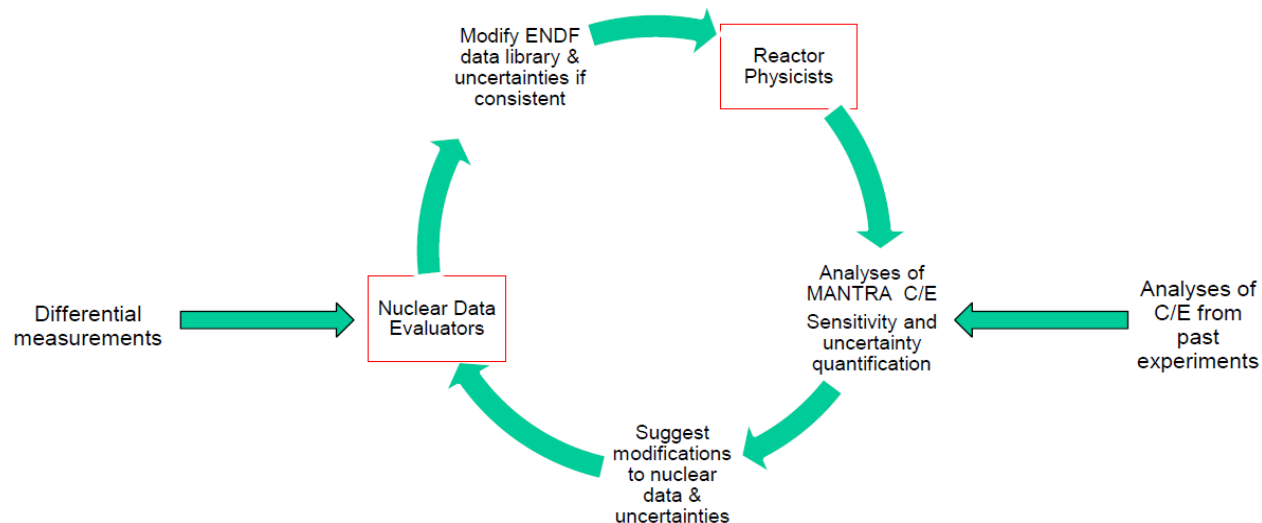
Even though we expect the MANTRA experimental program to be a success, there is already a need for a second phase (a MANTRA-2) of such a type of experiment. There are several reasons that justify this request. First there are several actinide samples that, for different reasons, have not been irradiated among others: Pu238, Pu241, and especially Cm-244 (irradiated only with thin filters). Moreover, at the time of the second campaign efficient mass separators should be available at INL. This should allow purifying samples of isotopes already irradiated in MANTRA and avoid one of the main concerns related to contamination from other isotopes, in the post irradiation analysis.

Finally, due to the limited room available in most cases only one sample per isotope (and in a couple of cases two) will be irradiated in MANTRA. In the PROFIL French experiments there were three and even six samples (PROFIL-2) of the same isotopes that were irradiated, the reason being that in certain cases in the post irradiation analysis, due to bad manipulation, some samples were contaminated. We, hopefully, can expect a low rate of failure for MANTRA, but, in case something happens, the MANTRA-2 campaign should provide an opportunity for repeating the compromised irradiation of some isotopes.

In complement to the MANTRA campaign a separate experimental program can be foreseen to be performed at the NRAD facility. The INL NRAD is a TRIGA reactor that has enough room to allow the presence of thick neutron filters (including U238 blocks) that will really simulate a large range of spectra going form thermal, epithermal, soft fast, and hard fast. Measurement of fission rate spectral indices using fission micro-chamber can allow to assess the knowledge on a vast range of actinides (major and minors). Moreover, reactivity sample oscillations measurements with apparatus that are been implemented at the ISU (Idaho State University) reactors (including open and closed loop) and easily installed at NRAD can be foreseen. Measurements of actinides samples in different spectra will be invaluable for the validation of cross sections useful for advanced fuel cycles.

9. REFERENCES

[1] ASTM International E 321 – 96 (Reapproved 2005), "Standard Test Method for Atom Percent Fission in Uranium and Plutonium Fuel (Neodymium-148 Method)"

[2] ISO, *Guide to the Expression of Uncertainty in Measurement*, International Organization for Standardization, Geneva, Switzerland, 1993. Several supplements have been published; see Bich, W., Cox, M. C., and Harris, P. M., "Evolution of the *Guide to the Expression of Uncertainty in Measurement,*" *Metrologia* 43, S161, 2006.

[3] Taylor, B. N., and Kuyatt, C. E., *Guidelines for Evaluating and Expressing the Uncertainty of NIST Measurement Results*, NIST Technical Note 1297, National Institute of Standards and Technology, Gaithersburg, MD, 1994; www.physics.nist.gov/cuu/Uncertainty/bibliography.html.

[4] ATR NSUF User Guide Manual (https://secure.inl.gov/atrproposal/documents/ATRUsersGuide.pdf)